LUND UNIVERSITY

Laser-Based Investigations of Combustion Phenomena in Gas Turbine Related Burners

Subash, Arman

2018

Document Version:
Publisher's PDF, also known as Version of record

Link to publication

Citation for published version (APA):
Subash, A. (2018). *Laser-Based Investigations of Combustion Phenomena in Gas Turbine Related Burners*. [Doctoral Thesis (compilation), Department of Physics]. Department of Physics, Lund University.

Total number of authors:
1

General rights
Unless other specific re-use rights are stated the following general rights apply:
Copyright and moral rights for the publications made accessible in the public portal are retained by the authors and/or other copyright owners and it is a condition of accessing publications that users recognise and abide by the legal requirements associated with these rights.
- Users may download and print one copy of any publication from the public portal for the purpose of private study or research.
- You may not further distribute the material or use it for any profit-making activity or commercial gain
- You may freely distribute the URL identifying the publication in the public portal

Read more about Creative commons licenses: https://creativecommons.org/licenses/

Take down policy
If you believe that this document breaches copyright please contact us providing details, and we will remove access to the work immediately and investigate your claim.

LUND UNIVERSITY

PO Box 117
221 00 Lund
+46 46-222 00 00

Laser-Based Investigations of Combustion Phenomena in Gas Turbine Related Burners

Arman Ahamed Subash

LUND UNIVERSITY

DOCTORAL DISSERTATION

by due permission of the Faculty of Engineering at Lund University, will be publicly defended on Friday, January 26, 2018, at 9:15 a.m. in the lecture hall Sal F, Department of Physics, Professorgatan 1, Lund, for the degree of Doctor of Philosophy in Engineering.

Faculty Opponent:
Professor Frédérik Grisch,
CORIA, INSA de Rouen,
Université de Rouen, France

Organization Lund University Division of Combustion Physics, Department of Physics PO Box 118, SE-221 00 LUND, Sweden	Document name: Doctoral Dissertation Date of issue: January 26, 2018 CODEN: LUTFD2/TFCP-208-SE
Author: Arman Ahamed Subash	Sponsoring organization:

Title: Laser-Based Investigations of Combustion Phenomena in Gas Turbine Related Burners

Abstract

Experiments were performed on various combustion devices to investigate the flames employing different optical measurement techniques under atmospheric pressure conditions. Non-intrusive laser-based techniques provided in-situ information concerning different parameters of the combustion process, with a high degree of temporal and spatial resolution. In the thesis work, different parameters of interest in combustion research, such as visualization of different intermediate combustion species and measurement of the flow velocity field, were studied by use of laser-induced fluorescence (LIF) and particle image velocimetry (PIV). The aim was to better understand the reaction and post-flame zone, flame stabilization, flame-anchoring position, as well as turbulent-flow interactions under different operating conditions, while varying the equivalence ratio, Reynolds number, burner geometry, and composition of fuel employed. Also, high-speed chemiluminescence imaging was used to investigate the dynamics of the flame. A large part of the thesis work involves experimental studies of the flame produced in a downscaled prototype 4th generation dry low emission (DLE) burner in connection with the development of the Siemens SGT-750 gas turbine burner. The burner consists of three concentrically arranged sections: a) an outer Main section, b) an intermediate section (Pilot) and c) a central pilot body termed the RPL (Rich-Pilot-Lean) section. Each of these sections is designed to be premixed and to enable the equivalence ratio to be varied for achieving optimal combustion. There is a Quarl, a diverging conical section located at the burner exit, used for expanding the flow area and holding the flame. Planar laser-induced fluorescence (PLIF) of OH and chemiluminescence imaging were employed for studying the flame at the burner exit. The primary combustion occurred inside the RPL section, whereas the main combustion was stabilized downstream of the burner throat. The main flame was anchored inside the Quarl and was elongated within the combustor. Both the main and the primary flames were stabilized by the swirling motion of the flow. Vortex breakdown and recirculation zones assisted the steady combustion process. Investigations were carried out to study how these three sections of the burner interact with one other and affect the main combustion process for altering the operating conditions in each section separately, using methane (CH_4) as fuel. It was found that the RPL-Pilot flame was mostly confined within the Quarl and played an essential role in flame stabilization and in locating the flame-anchoring position. The flame stabilization region moved downstream when the RPL equivalence ratio (ϕ) was changed from lean to rich conditions, whereas it moved upstream when the global ϕ and the Pilot ϕ was increased. The flame was investigated for the change in geometry that occurred by removing the Quarl to understand the effect of the Quarl on the flame stabilization. Significant changes in the flame characteristics were observed for sudden expansion of the flow at the burner exit when the Quarl was not present. Since without the Quarl the flame can expand radially without any constraints, the flame shortened at the burner exit under such conditions. For the global $\phi \geq 0.52$, outer recirculation zones in the flame were observed when the Quarl was absent, but they were not observed when the Quarl was present. Experiments were also performed to investigate the flame for the enrichment of hydrogen (H_2) in the methane (CH_4) fuel. Three H_2/CH_4 fuel mixtures, having ratios (volumetrically) of 0/100, 25/75, and 50/50, respectively, were studied. The characteristics of the flame changed with the addition of H_2 due to the greater diffusivity, higher reaction rate, and higher laminar burning velocity of H_2. The H_2 enrichment shortened the flame, and the flame stabilization zone moved further downstream. At a constant global ϕ for alternation of the RPL ϕ and the Pilot ϕ, the trends of the changes in the flame position and stabilization that occurred in 0/100 and 25/75 (expressed in the vol. fuel ratio) of the H_2/CH_4 fuel mixtures were similar. In addition, experiments were performed on two laboratory-scaled burners: a Triple Annular Research Swirler (TARS) and a CECOST swirl burner. These are generic burners that can simulate the characteristics of a gas turbine burner, regarding both the fuel injection and the flame stabilization. The hysteretic behavior of flashback and flash-forward were investigated on the swirl-stabilized flame of the TARS burner, using OH-PLIF, CH_2O-PLIF, high-speed OH* chemiluminescence and particle image velocimetry (PIV). Two hysteresis loops were identified both for flashback and flash-forward, one for lean mixtures and the other for rich mixtures. The impacts of the relevant parameters including the Reynolds number, equivalence ratio, fuel type, combustion chamber geometry, preheating and mixing tube protrusions were also investigated. It was found that the equivalence ratios at which rich and lean flashbacks occurred, approached stoichiometric condition with an increase in the Reynolds number. On the average, flashback events under lean conditions were significantly slower than not only the same events under rich conditions but also the flash-forward events. Confinement effects were found to be less critical in both the cases of flashback and flash-forward events. Finally, the stabilization, lean blowout limit, and flashback of the flame were investigated for the CECOST swirl burner, employing simultaneous OH-PLIF and CH_2O-PLIF as well as high-speed chemiluminescence imaging. The lean blowout limit was found to be nearly invariant for all measured Reynolds numbers. On the other hand, the flashback was found to approach around equivalence ratio ($\phi = 0.6$) at lower Reynolds numbers and at higher equivalence ratios when the Reynolds number was increased up to Re = 17000. With a further increase in the Reynolds number, no flashback was observed, even when the equivalence ratio was increased close to stoichiometry. In the combustion chamber, the flame was stabilized by creating a central recirculation and outer recirculation zones. At these higher Reynolds number (Re > 17000), the flame size was reduced, and the central recirculation zone became stronger inside the combustion chamber with an increase in equivalence ratio.

Key words: Combustion, Gas turbine, chemiluminescence, laser-based techniques, LIF, PIV, DLE, TARS, CH_4, H_2, OH, CH_2O, equivalence ratio, flame stabilization, LBO, Flash-back, RPL.

Classification system and/or index terms (if any)		
Supplementary bibliographical information	Language: English	
ISSN and key title ISSN 1102-8718	ISBN 978-91-7753-523-2	
Recipient´s notes	Number of pages: 214	Price:
	Security classification	

Distribution by: Arman Ahamed Subash, Div. of Combustion physics, Department of Physics, Lund University PO Box 118, SE-221 00 LUND, Sweden

I, the undersigned, being the copyright owner of the abstract of the above-mentioned dissertation, hereby grant to all reference sources permission to publish and disseminate the abstract of the above-mentioned dissertation.

Signature: Subash

Date: 2017-12-4

Laser-Based Investigations of Combustion Phenomena in Gas Turbine Related Burners

DOCTORAL THESIS

Arman Ahamed Subash

Division of Combustion Physics
Department of Physics

LUND 2018

LUND UNIVERSITY

pp i-81 © 2018 Arman Ahamed Subash
Paper I © 2015 by ASME
Paper II © 2016 by ASME
Paper III © 2016 by ASME
Paper IV © 2017 by ASME
Paper V © 2017 by ASME
Paper VI © 2017 Taylor & Francis
Paper VII © 2018 by ASME

Printed at Media Tryck AB, Lund, Sweden
December 2017

Lund Reports on Combustion Physics, LRCP-208
ISBN 978-91-7753-523-2 (print)
ISBN 978-91-7753-524-9 (pdf)
ISSN 1102-8718
ISRN LUTFD2/TFCP-208-SE

Arman Ahamed Subash
Division of Combustion Physics
Department of Physics
Lund University
P.O. Box 118
SE-221 00, Lund, Sweden

ISO 14001:2004 CERTIFICATION™
Intertek
MILJÖMÄRKT
341903
fti

To my parents and my family

Abstract

Experiments were performed on various combustion devices to investigate the flames employing different optical measurement techniques under atmospheric pressure conditions. Non-intrusive laser-based techniques provided in-situ information concerning different parameters of the combustion process, with a high degree of temporal and spatial resolution. In the thesis work, different parameters of interest in combustion research, such as visualization of different intermediate combustion species and measurement of the flow velocity field, were studied by use of laser-induced fluorescence (LIF) and particle image velocimetry (PIV). The aim was to better understand the reaction and post-flame zone, flame stabilization, flame-anchoring position, as well as turbulent-flow interactions under different operating conditions, while varying the equivalence ratio, Reynolds number, burner geometry, and composition of fuel employed. Also, high-speed chemiluminescence imaging was used to investigate the dynamics of the flame.

A large part of the thesis work involves experimental studies of the flame produced in a downscaled prototype 4th generation dry low emission (DLE) burner in connection with the development of the Siemens SGT-750 gas turbine burner. The burner consists of three concentrically arranged sections: a) an outer Main section, b) an intermediate section (Pilot) and c) a central pilot body termed the RPL (Rich-Pilot-Lean) section. Each of these sections is designed to be premixed and to enable the equivalence ratio to be varied for achieving optimal combustion. There is a Quarl, a diverging conical section located at the burner exit, used for expanding the flow area and holding the flame. Planar laser-induced fluorescence (PLIF) of OH and chemiluminescence imaging were employed for studying the flame at the burner exit. The primary combustion occurred inside the RPL section, whereas the main combustion was stabilized downstream of the burner throat. The main flame was anchored inside the Quarl and was elongated within the combustor. Both the main and the primary flames were stabilized by the swirling motion of the flow. Vortex breakdown and recirculation zones assisted the steady combustion process. Investigations were carried out to study how these three sections of the burner interact with one other and affect the main combustion process for altering the operating conditions in each section separately, using methane (CH_4) as fuel. It was found that the RPL-Pilot flame was mostly confined within the Quarl and played an essential role in flame stabilization and in locating the flame-anchoring position. The flame stabilization

region moved downstream when the RPL equivalence ratio (ϕ) was changed from lean to rich conditions, whereas it moved upstream when the global ϕ and the Pilot ϕ was increased. The flame was investigated for the change in geometry that occurred by removing the Quarl to understand the effect of the Quarl on the flame stabilization. Significant changes in the flame characteristics were observed for sudden expansion of the flow at the burner exit when the Quarl was not present. Since without the Quarl the flame can expand radially without any constraints, the flame shortened at the burner exit under such conditions. For the global $\phi \geq 0.52$, outer recirculation zones in the flame were observed when the Quarl was absent, but they were not observed when the Quarl was present. Experiments were also performed to investigate the flame for the enrichment of hydrogen (H_2) in the methane (CH_4) fuel. Three H_2/CH_4 fuel mixtures, having ratios (volumetrically) of 0/100, 25/75, and 50/50, respectively, were studied. The characteristics of the flame changed with the addition of H_2 due to the greater diffusivity, higher reaction rate, and higher laminar burning velocity of H_2. The H_2 enrichment shortened the flame, and the flame stabilization zone moved further downstream. At a constant global ϕ for alternation of the RPL ϕ and the Pilot ϕ, the trends of the changes in the flame position and stabilization that occurred in 0/100 and 25/75 (expressed in the vol. fuel ratio) of the H_2/CH_4 fuel mixtures were similar.

In addition, experiments were performed on two laboratory-scaled burners: a Triple Annular Research Swirler (TARS) and a CECOST swirl burner. These are generic burners that can simulate the characteristics of a gas turbine burner, regarding both the fuel injection and the flame stabilization. The hysteretic behavior of flashback and flash-forward were investigated on the swirl-stabilized flame of the TARS burner, using OH-PLIF, CH_2O-PLIF, high-speed OH* chemiluminescence and particle image velocimetry (PIV). Two hysteresis loops were identified both for flashback and flash-forward, one for lean mixtures and the other for rich mixtures. The impacts of the relevant parameters including the Reynolds number, equivalence ratio, fuel type, combustion chamber geometry, preheating and mixing tube protrusions were also investigated. It was found that the equivalence ratios at which rich and lean flashbacks occurred, approached stoichiometric condition with an increase in the Reynolds number. On the average, flashback events under lean conditions were significantly slower than not only the same events under rich conditions but also the flash-forward events. Confinement effects were found to be less critical in both the cases of flashback and flash-forward events. Finally, the stabilization, lean blowout limit, and flashback of the flame were investigated for the CECOST swirl burner, employing simultaneous OH-PLIF and CH_2O-PLIF as well as high-speed chemiluminescence imaging. The lean blowout limit was found to be nearly invariant for all measured Reynolds numbers. On the other hand, the flashback was found to approach around equivalence ratio ($\phi = 0.6$) at lower Reynolds

numbers and at higher equivalence ratios when the Reynolds number was increased up to Re = 17000. With a further increase in the Reynolds number, no flashback was observed, even when the equivalence ratio was increased close to stoichiometry. In the combustion chamber, the flame was stabilized by creating a central recirculation and outer recirculation zones. At these higher Reynolds number (Re > 17000), the flame size was reduced, and the central recirculation zone became stronger inside the combustion chamber with an increase in equivalence ratio.

Popular science

Combustion is inseparable from human life and cultural development; it is an innate part of both. Modern civilization relies very much on combustion for electricity production, transportation, heating, propulsion, and industrial processing. Different combustion devices, such as internal combustion engines, gas turbines, furnaces and burners of various sorts are being used for the control and utilization of combustion. Fossil fuel plays a vital role in meeting the energy consumption needs of the world. At present, fossil fuels account for approximately 81.4% of the world's total energy consumption. In the future, the demands placed on the primary energy supplies will increase along with population growth in order to maintain the same or progress living standards. The combustion of fossil fuels can also cause health and environmental hazards. Alongside the usual combustion products, such as water, carbon dioxide (CO_2), and heat energy, combustion also produces unintended pollutants. The emissions of carbon monoxide (CO), nitrogen oxides (NO_X), sulfur oxides (SO_X), and heavy metals from combustion are harmful due to their toxicity, and play a role in depletion of the ozone layer, in the creation of acid rain, as well as in greenhouse effects. The fossil fuel resources that are available are also limited. It is thus imperative to discover and make use of alternative energy sources as well as to optimize existing combustion technologies for maximizing fuel-burning efficiency and minimizing the emission of pollutants. Since CO_2 levels in the atmosphere also affect the environment adversely, increasing attention is being directed at research on the reduction of CO_2 impact and the use of CO_2-neutral fuel. A gas turbine is a combustion engine that can convert fuel to mechanical power. Then this mechanical power can be used for producing electric power and generating thrust in a jet aircraft. The gas turbine consists of three primary sections: a compressor, a combustor, and a turbine. The bulk air is compressed in the compressor section. The compressed air then enters the combustor, where it mixes with fuel so that combustion occurs. Finally, the hot combustion products that are produced expand through the turbine section. The combustor is an essential component of the gas turbine operations. For designing a stationary gas turbine combustor, various features, such as the use of safe and reliable operations avoiding instabilities, a high level of combustion efficiency, a low level of pollutant emissions and a high level of fuel flexibility, are important. To be able to achieve these, profound knowledge and a deeper understanding of the combustion process are imperative. Combustion is a complicated process that involves enormous numbers of chemical reactions and a variety of physical processes that take place in different time and length scales. In practical devices, such as gas turbines and internal combustion engines, the combustion process is even more complicated since most of the flows are turbulent there. In turbulent combustion, flow velocity, species concentration, and temperature vary arbitrarily both in time and space. Sufficiently rapid and sensitive measurement techniques are required to be able to observe what is happening in different parts and at various time scales during the combustion process. Laser-based diagnostics can play a vital role because of its high temporal and spatial resolutions. Information about various parameters, such as the temperature, species concentration, and velocity field, can be achieved without disturbing the chemical process or flow dynamics.

In the thesis, experiments were performed on several combustion devices associated with gas turbines for studying the flames by use of different laser-based measurement techniques. A prototype 4th generation dry low emissions (DLE) burner developed by Siemens Industrial Turbomachinery is one of the burners that were tested. It consists of three concentric sections. The ability to vary the ratio of fuel to air in each section enables the burner to achieve optimal combustion. In addition, two laboratory-scaled burners, namely a TARS (Triple Annular Research Swirler) and a CECOST (the Centre for Combustion Science and Technology) swirl burner, were used in the flame investigations. These two burners have simplified geometries and can simulate the characteristics of a gas turbine burner, regarding both the fuel injection and the flame stabilization involved.

Optical techniques, such as laser-induced fluorescence (LIF) and chemiluminescence imaging, were employed to investigate the turbulence-flame interactions and flame stabilization. LIF is one of the most widely used techniques in the field of combustion research. It involves the target atoms and molecules being excited from a lower to a higher energy state by absorbing light of a specific wavelength. The energy of the wavelength selected is equal to the difference in energy between these two energy states. After excitation, the atoms and/or molecules involved can de-excite to lower energy levels through spontaneous emission, and this spontaneous emission is termed fluorescence. The fluorescence signals can provide spatial and quantitative information regarding different intermediate species, as well as the temperature distribution in the combustion zone. The absorption and fluorescence wavelengths are unique to specific species or radical, making the technique useful for studying a particular chemical species selectively. OH, and CH_2O are intermediate species in the combustion process and indicating the various states of the combustion process. Visualization of the species in two dimensions achieved by use of the LIF techniques can provide detailed information regarding the flame characteristics. Chemiluminescence imaging provides information about the position, size, and shape of the flame. Chemiluminescence imaging at a high repetition rate is also useful for understanding the dynamic behavior of the flame. Chemiluminescence is the emission of radiation when the atoms and molecules are excited by extracting the excess energy from the chemical reactions and returning to a lower energy state. The wavelength of the radiation that is emitted tends to be characteristic of the particular molecule involved. A large part of the thesis work consists of experimental studies of the flame produced in a prototype DLE burner in which OH-LIF and chemiluminescence imaging were employed. The investigations were carried out for studying the flames under atmospheric pressure conditions while altering the operating conditions in different sections of the burner, changing the burner geometry and altering the composition of the fuel employed. For the TARS burner, the investigations were carried out to better understand how the degree of turbulence of the flow, changes in the burner geometry, and alteration of the fuel affect the undesired extinction of the flame. Finally, the flame stabilization mechanisms and flame characteristics of the CECOST burner were investigated by use of simultaneous OH- and CH_2O-LIF, as well as high-speed chemiluminescence imaging.

List of papers

I. **Subash, A. A.,** Whiddon, R., Kundu, A., Collin, R., Klingmann. J., & Aldén, M., "Flame Investigation of a Gas Turbine Central Pilot Body Burner at Atmospheric Pressure Conditions Using OH PLIF and High-Speed Flame Chemiluminescence Imaging",
In Proceedings of the ASME Gas Turbine India Conference, 2015, GTINDIA2015-1212

II. **Subash, A. A.,** Kundu, A., Collin, R., Klingmann. J., & Aldén, M., "Laser-Based Investigation on a Dry Low Emission Industrial Prototype Burner at Atmospheric Pressure Conditions",
In Proceedings of the ASME Turbo Expo 2016, Volume 4B: Combustion, Fuels and Emissions, GT2016-57242

III. Kundu, A., **Subash, A. A.,** Collin, R., & Klingmann. J., "Flame Stabilization and Emission Characteristics of a Prototype Gas Turbine Burner at Atmospheric Conditions",
In Proceedings of the ASME Turbo Expo 2016, Volume 4B: Combustion, Fuels and Emissions, GT2016-57336

IV. **Subash, A. A.,** Kundu, A., Collin, R., Klingmann. J., & Aldén, M., "Experimental Investigation of the Influence of Burner Geometry on Flame Characteristics at a Dry Low Emission Industrial Prototype Burner at Atmospheric Pressure Conditions",
In Proceedings of the ASME Turbo Expo 2017, Volume 4A: Combustion, Fuels and Emissions, GT2017-63950

V. **Subash, A. A.,** Kundu, A., Collin, R., Klingmann. J., & Aldén, M., "Hydrogen Enriched Methane Flame in a Dry Low Emission Industrial Prototype Burner at Atmospheric Pressure Conditions",
In Proceedings of the ASME Turbo Expo 2017, Volume 4A: Combustion, Fuels and Emissions, GT2017-63924

VI. Szasz, R.Z., **Subash, A. A.,** Lantz, A., Collin, R., Fuchs, L., & Gutmark, E.J., "Hysteretic Dynamics of Flashback in a Low-Swirl Stabilized Combustor",
Journal Combustion Science and Technology Volume 189, 2017 – Issue 2

VII. Yu, S., **Subash, A. A.,** Liu, X., Liu, X., Hodzic, E., Szasz, R.Z., Bai, X.S., Li, Z.S., Collin, R., Aldén, M., & Lörstad, D., "Numerical and Experimental Investigation of the Flame Structures in a New Lab-Scale Gas Turbine Swirl Burner",
ASME Turbo Expo 2018 (submitted)

Related Work

A. Kundu, A., **Subash, A. A.,** Collin, R., & Klingmann. J., "Fuel Flexibility of a Multi-Staged Prototype Gas Turbine Burner",
In Proceedings of the ASME Turbo Expo 2016, Volume 4B: Combustion, Fuels and Emissions, GT2017-64782

B. Kundu, A., **Subash, A. A.,** Collin, R., & Klingmann. J., "Pilot-Pilot Interaction Effects on a Prototype DLE Gas Turbine Burner Combustion",
In Proceedings of the ASME Turbo Expo 2016, Volume 4B: Combustion, Fuels and Emissions, GT2016-57338

C. Kundu, A., **Subash, A. A.,** Collin, R., & Klingmann. J., "Experimental and Numerical Investigation of a Prototype Low NOx Gas Turbine Burner",
In Proceedings of the ASME Power Conference, 2016, POWER2016-59592

D. Lantz, A., Larfeldt, J., Ehn, A., Zhu, J., **Subash, A. A.,** Nilsson, E. J.K., Li, Z., and Aldén, M., "Investigation of Ozone Stimulated Combustion in the SGT-800 Burner at Atmospheric Conditions",
In Proceedings of the ASME Turbo Expo 2016, Volume 4A: Combustion, Fuels and Emissions, GT2016-57111

E. Kundu, A., Whiddon, R., **Subash, A. A.,** Collin, R., & Klingmann. J., "Operability and performance of central (Pilot) stage of an industrial prototype burner",
In Proceedings of the ASME Power Conference, 2015, POWER2015-49449

F. Kamran, F., Abildgaard, O. H. A., **Subash, A. A.,** Andersen, P. E., Andersson-Engels, S., and Khoptyar, D., "Computationally effective solution of the inverse problem in time-of-flight spectroscopy", *Optics Express, 2015, Vol. 23, Issue 5, pp. 6937-6945*

G. Khoptyar, D., **Subash, A. A.,** Johansson, S., Saleem, M., Sparén, A., Johansson, J., and Andersson-Engels, S., "Broadband photon time-of-flight spectroscopy of pharmaceuticals and highly scattering plastics in the VIS and close NIR spectral ranges", *Optics Express, 2013, Vol. 21, Issue 18, pp. 20941-20953*

H. Abildgaard, O. H. A., **Subash, A. A.,** Nielsen, F. D., Dahl, A. B., Skytte J. L., Andersson-Engels, S., and Khoptyar, D., “Spectral characterization of dairy products using photon time-of-flight spectroscopy", *Journal of Near Infrared Spectroscopy, 2013, Volume 21 Issue 5, Pages 375–383*

Abbreviations

C_2	Carbon
CECOST	The Centre for Combustion Science and Technology
CFD	Computational fluid dynamics
CH_2O	Formaldehyde
CH_4	Methane
CIVB	Combustion-induced vortex breakdown
CO	Carbon monoxide
CO_2	Carbon dioxide
CRZ	Central recirculation zone
DLE	Dry low emission
FB	Flashback
FF	Flash-forward
H_2	Hydrogen
HC	Hydrocarbon
HCN	Hydrogen cyanide
ICCD	Intensified charge coupled device
ISL	Inner shear layer
LBO	Lean blowout
LDV	Laser Doppler velocimetry
LES	Large eddy simulation
LIF	Laser-induced fluorescence
MCP	Microchannel plate
NG	Natural gas
NO_X	Nitrogen oxides
OH	Hydroxyl
OSL	Outer shear layer
ORC	Outer recirculation zone
PCA	Principal component analysis
PDM	Probability density map
PFR	Pilot fuel ratio
PIV	Particle image velocimetry
PLIF	Planar LIF
POD	Proper orthogonal decomposition
RPL	Rich-Pilot-Lean
RET	Rotational energy transfer
SNR	Signal-to-noise ratio
SGT	Siemens gas turbine
SO_X	Sulfur oxides
T/C	Thermocouple
TARS	Triple annular research swirler
UV	Ultraviolet
VET	Vibrational energy transfer

Nomenclature

A_{21}	Einstein coefficient for spontaneous emission
B	Einstein coefficient for absorption and stimulated emission
c	Speed of light
c_i	Eigenvectors
D	Burner nozzle diameter
D_f	Thermal diffusivity
d	Displacement
Da	Damköhler number
E_i	Energy level
$f_\#$	Focal length
$F(r)$	Field distribution
g_i	Time coefficient
h	Planck's constant
I_v	Laser spectral irradiance
K	Kelvin
Ka	Karlovitz number
l_0	Characteristic length scale of eddy
m_i	Molar mass of the molecules
N_i	Population of atoms or molecules
P	Pressure
P_i	Predissociation rate constant
$P(x)$	Line-of-sight integral projection data
Q_{21}	Collisional quenching rate constant
Re	Reynolds number
S	Entropy
S_f	Fluorescence signal
S_L	Laminar flame speed
t	Time
T	Temperature
U	Data set
u	Characteristic velocity
V	Volume
W_{2i}	Photoionization rate constant
v	Photon frequency
v''	Ground electronic state
v'	First excited electronic state
δ_L	Flame thickness
τ	Residence time
τ_f	Fluorescence lifetime
τ_i	Characteristic time scale of eddy
η	Kolmogorov eddy length
Ω	Collection solid angle
Ψ_i	Eigenfunctions
ϕ	Equivalence ratio
λ	Eigenvalue

Contents

Chapter 1

Introduction

A role of combustion in aiding and supporting various aspects of human life started at the point in time when early human beings learned to control fire for their survival and it has continued in various ways up to the present. In many aspects of our lives, such as heating, transportation, propulsion, generation of electricity and industrial processing, combustion plays a highly important role. For a wide variety of applications, remarkable technical advancements have taken place during the last few centuries, in particular, in being able to utilize combustion in very much of a controlled manner. Internal combustion engines, gas turbines, furnaces and burners of different types are being used for controlling and utilizing combustion. Such differing setups as those used in small auxiliary power generation units of airplanes or in city-wide power generation facilities involve the combustion of various types of fuels. Although renewable energy sources can be the potential alternatives of the use of fossil fuels, the shift from the use of fossil fuels to the use of renewable energy sources does not currently appear very promising. At present, the fossil fuels (coal, oil, gasoline and natural gas) account for approximately 81.4 % of the world's total energy consumption [1]. Fossil fuel will surely be a significant energy source for several decades to come, even though the resources are limited. The combustion of fossil fuels does not entirely lack negative aspects. It can cause harm to human health and the environment. The emissions of NO_X, SO_X, CO and heavy metals can be hazardous, due to their toxicity, and are responsible for the depletion of the ozone layer, for acid rain, and for greenhouse effects. Also, the primary combustion product, CO_2, contributes to global warming [2]. For preserving a healthy and clean environment, legislative mandates for minimizing the emission of pollutants are gradually becoming stricter. It thus becomes imperative to find alternative energy sources and optimize the existing combustion technologies in order to minimize the emission of pollutants, while maintaining a high level of fuel-burning efficiency. Profound knowledge and a deeper understanding of the combustion process are indispensable for controlling combustion sufficiently and developing combustor design. Combustion is a complicated process that involves an enormous number of chemical reactions and a wide variety of physical phenomena occurring on different scales of time and length. In practical devices, such as gas turbines and internal combustion engines, this process is even more complicated since most of the flows are turbulent there. Turbulence accelerates the combustion process by enhancing the mixing of fuel and air, and it enables a flame and combustor to be quite small in size for a given load and power output to be achieved. Turbulence is not a stable process, and in this process, the instantaneous velocities exhibit random fluctuations. In turbulent combustion, the flow velocity, species concentration, and temperature fluctuate arbitrarily, both in terms of time and of space. The instabilities that appear in combustion can also be caused by the flame-turbulence interactions together with acoustic waves. Different species interact with the turbulence within a continuous spectrum of both the time and the length scale. Consequently, temporally and spatially resolved techniques are essential for obtaining a proper understanding of different combustion phenomena. Laser-based measurement techniques are thus very advantageous in the field of combustion research since these have both high temporal and high spatial resolutions. Various parameters, such as the temperature, species concentration, and velocity field, can be achieved both non-intrusively and remotely. Laser diagnostics can also be used for species-selective studies involving the use of selected wavelengths. In addition, the computational fluid dynamics (CFD) of reacting and non-reacting flows, as well as chemical models, can be useful tools for obtaining a better understanding of the combustion process through modeling of the turbulent flow and combustion. Advanced optical measurement techniques together with sophisticated data analysis tools can provide opportunities to validate numerical simulations and achieve a detailed understanding of the processes. Information regarding temperature, intermediate species, velocity profile and combustion dynamics are valuable for designing as well as producing efficient and clean combustion engines.

As a form of technology, a gas turbine plays a vital role in the field of power generation. It is a kind of combustion engine that can convert fossil fuels to mechanical power. Then this mechanical power can be used to drive a generator to produce electrical power. In addition to power generation, gas turbines are also widely used in the aerospace/aviation industry, marine propulsion, and different military applications. The combustion chamber is an essential component of gas turbine operations. For the designing of stationary gas turbine combustors, it is essential to achieve safe and reliable operations within the entire loading range avoiding instabilities, a high level of combustion efficiency, a low level of emission pollutants and a high degree of fuel flexibility. The lean premixed approach of combustion is well-known for operating stationary gas turbines. It provides low combustion temperatures and limits thermal NO_X creation pathway [3, 4]. However, the lean premixed mode of operations may lead the combustor towards unstable conditions that induce local extinction, poor combustion efficiency, and combustion instabilities [5]. The addition of a diffusion pilot flame and a pre-chamber combustor in burner design can help to stabilize lean premixed combustion [6] and ensure a lower NO_X emission level [7]. In the thesis, a significant part of the work involves experimental studies carried out on a prototype 4th generation dry low emission (DLE) burner under atmospheric pressure conditions. This burner was developed by Siemens Industrial Turbomachinery [8] for minimizing NO_X and CO emissions. Investigations performed on this burner concern development of the Siemens SGT-750 gas turbine burner. The prototype test burner has three stages in which a pre-chamber combustor is included. The pre-chamber combustor, termed the RPL (rich-pilot-lean), produces heat and chemically active species or radicals [9] for stabilizing the main flame at lean operating conditions close to lean blowout (LBO) limits and reducing the emission of pollutants. The flame is stabilized by a swirling induced vortex breakdown mechanism. Investigations were performed to study both the flame and emission under atmospheric pressure conditions while verifying different parameters (such as the equivalence ratio, flow velocity, and bulk air temperature) in three stages, changing the burner geometry, and altering the fuel composition employed. Planar laser-induced fluorescence (PLIF) of OH and flame chemiluminescence imaging were employed for studying the formation of reaction zones, turbulence-flame interactions, and flame stabilization at the burner exit. In addition, two laboratory-scaled burners, namely a TARS (Triple Annular Research Swirler) and a CECOST swirl burner were employed for flame investigations. These two burners have simplified geometries and can simulate the characteristics of a gas turbine burner, regarding both the fuel injection and the flame stabilization. The hysteretic behavior of flashback and flash-forward was investigated in methane and natural gas flames of the TARS burner using OH-PLIF, CH_2O-PLIF, high speed OH* chemiluminescence imaging and particle image velocimetry (PIV). Finally, the flame stabilization, lean blowout limits, and flashback were investigated on the CECOST swirl burner, employing simultaneous OH-PLIF and CH_2O-PLIF as well as high-speed chemiluminescence imaging.

The outline of the thesis is as follows. Chapter 2 presents a survey of the experimental measurement techniques employed in the thesis work. It provides a brief introduction to the fundamental principles of the measurement techniques employed. Chapter 3 deals with the relevant measurement equipment, in particular, the laser sources and the detectors used in the experiments and an overview of the data processing methods involved. A general introduction to gas turbine combustion and the specific combustion devices used in the investigations is given in Chapter 4. Chapter 5 presents brief descriptions of the application of the different techniques to the various combustion devices employed as well as the results of the investigations as a whole. Finally, the summary of the work and future considerations are provided in Chapter 6. The published papers included in the thesis are attached at the very end.

Chapter 2

Measurement techniques

In the thesis, different optical measurement techniques were employed for combustion studies in various combustion devices. Visualization of the intermediate species in the combustion was achieved by use of laser-induced fluorescence (LIF) technique. Chemiluminescence imaging provided the information regarding the size and shape of the flame as well as the flame dynamics, whereas the flow field was investigated using particle image velocimetry (PIV). The objective was to achieve a better understanding of the reaction and post flame zones, flame stabilization, flame-anchoring position and turbulent-flame interactions under different combustion conditions. This chapter presents an overview of the basic principles of the various measurement techniques involved.

2.1 Laser-induced fluorescence

The continuous development of different laser sources, detectors, and optics has brought about the LIF technique as a well-established and widely used optical measurement tool for combustion investigations. This technique can provide both high temporal and spatial resolutions in studies of the different species present at low concentrations and in different temperature distributions in the flame. Species distributions are beneficial for understating the flame structures, such as the flame front, the post-flame region, as well as the burnt and un-burnt regions. They also provide information regarding the dynamics of the turbulent-flame interactions in the combustion process.

All atoms, whether alone or in molecules, consist of a nucleus and a cloud of electrons orbiting the nucleus. The electrons spin around the nucleus in various orbits or shells of discrete energies. These shells build up energy levels that are specific to the species involved. The energy level of an electron depends upon the distance between the nucleus and the shell in which the electron is orbiting. The larger the gap, the higher the electron energy level is. Transitions of the electrons between these discrete levels can occur through the absorption or (either spontaneous or stimulated) emission of photons. An atom or molecule, or its electrons, can be excited from a lower to a higher energy level by the absorption of a photon of specific energy and can be de-excited from a higher to a lower energy level through the emission of a photon. If the excited electrons emit photons in random directions, there is no phase relationship between the photons, and the emission process is referred to as a spontaneous one. In a stimulated emission process, an electron is induced by the presence of a photon to de-excite from a higher to a lower energy level. In the absorption and the stimulated emission processes, the photon energy is equal to the energy separation between the two participating energy levels.

Laser-induced fluorescence is a resonant technique. In this technique, the atoms or molecules involved are excited from a lower to a higher energy level by laser excitation, the wavelength of the photon being chosen to match the energy separation between the two energy levels. After excitation, several processes can take place. The atom or molecule can go back to the lower energy level through stimulated emission induced by laser radiation. It can instead absorb an additional photon and be excited to a higher energy level, resulting in photoionization. If it is a molecule, it can dissociate into smaller fragments. Its internal energy can also be altered by inelastic collisions with surrounding atoms or molecules, producing rotational energy transfer (RET), vibrational energy transfer (VET), and/or electronic energy transfer. The molecule can also lose energy due to collision(s) with other molecules or atoms that lead(s) to a non-radiative de-excitation. Finally, the atom or molecule can spontaneously de-excite to lower energy levels and emit photons, these being termed fluorescence signals. The light that is emitted may have either the same or a longer wavelength than the excitation wavelength. In performing LIF measurements in combustion environments, this shift is used to avoid or to suppress interference from laser-scattered light. LIF features both high spatial resolution (up to 40 μm) and high temporal resolution (around 10 ns) [10].

The application of laser-based diagnostics to combustion has been thoroughly documented by Eckbreth [11] and in review articles by Kohse-Höinghaus [12], and the various applications of LIF in combustion diagnostics can be found in Daily or Stepowski [13, 14]. For describing the basis of LIF, a simple two-energy level model shown in Fig. 2.1 can be considered [15]. The energy and the population at the lower level are E_1 and N_1, respectively, and those at the upper level are E_2 and N_2. The terms b_{12} and b_{21} are the rate constants for absorption and for stimulated emission, respectively.

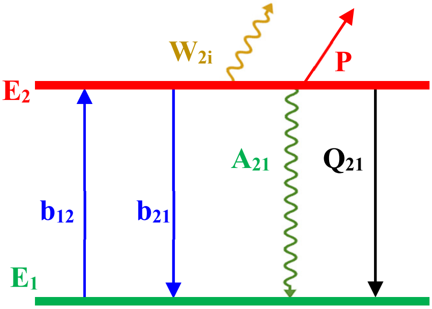

Figure 2.1: An energy level diagram for a two-level fluorescence model.

If B is the Einstein coefficient for absorption and stimulated emission, the rate constants are related through

$$b = \frac{BI_\nu}{c} \tag{2.1}$$

where I_ν is the laser spectral irradiance and c is the speed of light. The rate equations for the populations of the two energy levels [11] are given by

$$\frac{dN_1}{dt} = -N_1 b_{12} + N_2(b_{21} + A_{21} + Q_{21}) \tag{2.2}$$

$$\frac{dN_2}{dt} = N_1 b_{12} - N_2(b_{21} + A_{21} + Q_{21} + W_{2i} + P_i) \tag{2.3}$$

here, A_{21} is the Einstein coefficient for spontaneous emission, W_{2i} is the photoionization rate constant, Q_{21} is the collisional quenching rate constant, and P_i is the predissociation rate constant. Collisional quenching, photoionization and predissociation are non-radiative processes that reduce the strength of the fluorescence signal. Most of the excited states are not predissociative, and photoionization can be avoided by choosing a sufficiently low laser energy level. Accordingly, the predissociation and the photoionization rate constants can be neglected. Assuming that the population of the excited state prior to excitation is negligible and that the two energy levels represent a closed system with no population loss, the following Eq. can be written

$$\frac{dN_1}{dt} + \frac{dN_2}{dt} = \frac{d}{dt}(N_1 + N_2) = 0 \tag{2.4}$$

which gives

$$(N_1 + N_2) = N = N_1^0 \tag{2.5}$$

where the zero superscript identifies the initial population level N_1, and N is the total population. Eq. 2.3 has an algebraic solution if a steady-state for the processes considered in Fig. 2.1 is established and if Eq. 2.4 holds. The equation can be solved for N_2 by eliminating N_1, when the initial condition is $N_2\ (t = 0) = 0$, the solution then being

$$N_2(t) = \frac{N_1^0 b_{12}(1 - e^{-(b_{12}+b_{21}+A_{21}+Q_{21})t})}{(b_{12} + b_{21} + A_{21} + Q_{21})} \tag{2.6}$$

After a short period (~1 ns), the system reaches the steady-state for the processes as shown in Fig 2.1. Eq. 2.6 can then be written as

$$\begin{aligned} N_2 &= \frac{N_1^0 b_{12}}{(b_{12} + b_{21})\left(1 + \frac{A_{21} + Q_{21}}{b_{12} + b_{21}}\right)} \\ &= \frac{N_1^0 B_{12}}{(B_{12} + B_{21})\left(1 + \frac{I_{sat}^{\nu}}{I_\nu}\right)} \end{aligned} \tag{2.7}$$

where the saturation spectral irradiance I_{sat}^{ν} is defined as

$$I_{sat}^{\nu} = \frac{(A_{21} + Q_{21})c}{B_{12} + B_{21}} \tag{2.8}$$

The fluorescence rate is converted to a total fluorescence signal power S_f by temporal integration over the duration of the laser pulse. The fluorescence signal power, which is proportional to $N_2 A_{21}$, can be written as

$$S_f = h\nu\frac{\Omega}{4\pi}laN_2A_{21} = h\nu\frac{\Omega}{4\pi}laN_1^0\frac{B_{12}}{(B_{12} + B_{21})}\frac{A_{21}}{\left(1 + \frac{I_{sat}^{\nu}}{I_\nu}\right)} \tag{2.9}$$

here, h is the Planck's constant, ν is the emitted photon frequency, Ω is the solid angle of collection, l is the axis from which the fluorescence is collected, and a is the focal area of the laser beam. The strength of the fluorescence signal is proportional to the initial population of the energy level at which the excitation takes place, which is related to the total species population via the Boltzmann distribution. For low levels of laser irradiance, $I_\nu \ll I_{sat}^{\nu}$ Eq. 2.9 can be rewritten as

$$S_f = \frac{h\nu}{c}\frac{\Omega}{4\pi} laN_1^0 B_{12} I_\nu \frac{A_{21}}{A_{21} + Q_{21}} \tag{2.10}$$

In the *linear regime,* the fluorescence signal (S_f) is linearly proportional to the laser irradiance. S_f is proportional to the number of molecules of the probed species contained in the measurement volume, laN_1^0. The term $\frac{A_{21}}{A_{21}+Q_{21}}$ is the fluorescence quantum yield, which is usually much smaller than unity since quenching is the dominant process and the quenching rate constant Q_{21} then becomes more significant in number. It also means that most of the excited molecules lose their excitation energy through non-radiative processes. For performing measurements quantitatively, it is required that the quenching rate constant Q_{21}be estimated. Determination of it is not an easy task since Q_{21} is a function of the pressure, temperature, and molecular collisional partners. One approach to determine Q_{21} is to measure the temperature and the dominant quenching species and to calculate the quenching correction needed for the data [16, 17]. Another approach is to measure the lifetime and hence the quenching rate [18, 19]. The lifetime (τ_f) is related to the quenching rate constant, as shown in Eq. 2.11.

$$\tau_f = \frac{1}{(A_{21} + Q_{21})} \tag{2.11}$$

here A_{21} is assumed to be known. In steady flows and in laminar flames, these approaches work very well since it is possible to carry out sequential and/or time average measurements. This method can also be used in a turbulent environment if the signal-to-noise ratio is sufficiently high. A strategy for avoiding quenching corrections can be to measure the *saturated regime,* in which the laser excitation irradiance is always higher than the saturation irradiance, i.e., $I_\nu \gg I_{sat}^\nu$. In this regime, Eq. 2.9 can be rewritten as

$$S_f = h\nu\frac{\Omega}{4\pi} laN_1^0 A_{21} \frac{B_{12}}{B_{12} + B_{21}} \tag{2.12}$$

here, the fluorescence signal (S_f) is neither dependent on the laser excitation irradiance nor on the quenching rate constant. In this regime, the fluorescence signal can be maximized. However, it can be difficult to achieve saturation in the wings of a focused laser beam or during the entire duration of a laser pulse. It is also tricky to achieve a sufficiently high laser excitation irradiance for all wavelengths. For getting rid of quenching corrections, other alternatives are photoionization LIF and predissociative LIF. In photoionization LIF, a second laser that overlaps the laser causing fluorescence is used to photoionize the molecule. Then W_{2i} dominates for the loss from the excited state. In predissociative LIF, the molecule is excited to a predissociative state where the loss from the excited state is dominated by P_i and $P_i \gg Q_i > A_i$. Predissociative

LIF can only be performed at low to atmospheric pressures, whereas at higher pressures, $Q_i \approx P_i$ and the quenching cannot be neglected. Both predissociative LIF and photoionization LIF suffer from low fluorescence efficiency and low species detection capability. For achieving quantitative information, LIF in the linear regime is still the most widely applied approach in the field of combustion diagnostics. LIF is also frequently used to visualize a two-dimensional distribution of different species in a combustion environment. In the thesis, the flame characteristics were investigated employing OH-PLIF and CH_2O-PLIF in the *linear regime*. All comparisons of the results were performed qualitatively.

2.1.1 Hydroxyl (OH) LIF

OH-PLIF measures can provide qualitative information regarding the OH radical distribution in the flame that can be observed along the laser sheet. OH is an intermediate species in combustion and is formed in the important reaction zone by fast two-body reactions following

$$H + O_2 \rightarrow OH + O \tag{2.13}$$

$$O + H_2 \rightarrow OH + H \tag{2.14}$$

Then it initiates the oxidation of hydrocarbon fuels by removing hydrogen atoms from the fuel molecules. The OH radical concentration remains high in the reaction zone, and it slowly decreases in the hot post-flame region [20]. Therefore it acts as a marker both for the flame front and post-flame regions. The high-intensity region indicates the position of the OH radicals that are formed in the flame front or have been convected a relatively short distance. OH is a spectroscopically well-characterized radical. (a) $A^2\Sigma^+(v' = 0) \leftarrow X^2\Pi(v'' = 0)$ and (b) $A^2\Sigma^+(v' = 1) \leftarrow X^2\Pi(v'' = 0)$ are the two most frequently used schemes for performing OH-LIF measurement. The terms $v'$and v''denote vibrational levels in the first excited electronic state and the ground state, respectively. Transition (b) is commonly used for excitation, the transition (a) being for the collection of fluorescence light. Fig. 2.2 shows a schematic diagram of the excitation and fluorescence scheme for the OH radical. After excitation, collisions with surrounding species lead to a redistribution of the energy level population through vibrational energy transfer (VET) and rotational energy transfer (RET). These processes bring molecules from the pumped level that has been selected to neighboring rotational and vibrational levels. Accordingly, many different rotational levels in $v' = 0$ are populated, the fluorescence thus being emitted from several different rotational levels and containing many different wavelengths.

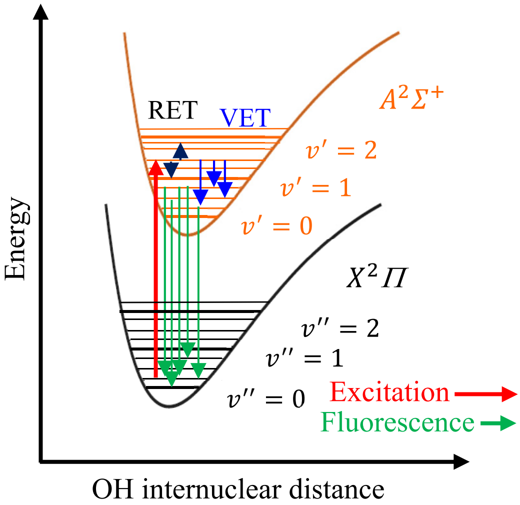

Figure 2.2: An energy-level diagram for the ground and first electronically excited states in the OH radical.

In the working frame of the thesis, planar laser-induced fluorescence (PLIF) of OH measurement was carried out by exciting the $Q1(8)$ transition of the OH radical with use of a 283 nm laser sheet for the $A^2\Sigma^+(v' = 1) \leftarrow X^2\Pi(v'' = 0)$ scheme. A frequency-doubled (532 nm) Nd: YAG laser was used to pump a tunable dye laser (operating with the use of Rhodamine 590). The output of the dye laser was frequency doubled and tuned to the $Q1(8)$ transition. The $Q1(8)$ transition was chosen since it shows strong fluorescence and is nearly temperature-insensitive over the flame temperature region from 1400 K to 2500 K [21]. The resulting OH fluorescence at around 310 nm for the $A^2\Sigma^+(v' = 0) \leftarrow X^2\Pi(v'' = 0)$ scheme was collected perpendicular to the laser sheet by use of an ICCD camera.

2.1.2 Formaldehyde (CH_2O) LIF

Formaldehyde is an intermediate species in the preheating phase of hydrocarbon combustion [2]. It is formed in an early phase of combustion by means of low-temperature reactions when hydrocarbon starts to oxidize. It is consumed in the reaction zone and serves as a well-suited tracer species of cool-flame regions. The first measurements of formaldehyde in a flame using laser-induced fluorescence (LIF) were performed by Harrington and Smyth [22]. The product of the formaldehyde and the OH concentration was shown to provide spatial information concerning the intermediate species HCO, which in turn is a tracer for the flame front via heat release [23]. The theoretical description of formaldehyde spectroscopy is complicated because of different vibrational possibilities, as well as compact rotational line structures and geometric changes of molecules in excited states [24]. The formaldehyde molecule has several absorption bands suitable for excitation within the wavelength range of 270 nm to 360 nm. The higher vibrational states are populated as the temperature increases. This makes the absorption spectrum more complicated. In the present work, CH_2O-PLIF was performed by exciting the formaldehyde molecules with a laser sheet of 355 nm wavelength, which involve the 4_0^1 band of the electronic transition band $A^1A_2 \rightarrow X^1A_1$. The same excitation wavelength for CH_2O-LIF was used in studies [10, 25-27]. The 355 nm wavelength is the third harmonic produced by a standard Nd: YAG laser. The spectrum of the fluorescence is broadband, and the fluorescence signal is collected in the wavelength range of 360 – 600 nm. Despite 355 nm having a low absorption coefficient and possible interference of the fluorescence signal by other species, such as PAHs, this wavelength is desirable because of its accessibility through frequency conversion of the fundamental mode of a Nd: YAG laser, which is the most frequently employed laser system for combustion diagnostics.

2.2 Flame chemiluminescence

Chemiluminescence is the emission of radiation when the atoms and molecules are excited by extracting the excess energy from a chemical reaction and then returning to a lower energy state. The wavelength of the radiation that is emitted is characteristic of the particular molecule involved. For complicated molecules, the radiation spectra appear to be continuous, whereas for some simple (diatomic) molecules the spectrum is rather simple and exhibits one dominant peak and a few relatively weak secondary peaks. CH^* and C_2^* show main peaks at 431 nm and 513 nm in the blue-green region, whereas OH^* shows a peak at 310 nm in the UV region. Since the strength of the radiation at a specific wavelength observed in the flame is proportional to the concentration of the associated excited molecule, the measurement of the radiation can indicate the concentration of the excited molecule. The excited molecule can also lose its excess energy through non-reactive collisions or reactions with other molecules. A collision that occurs without emitting light is called a quenching collision. Since chemiluminescence occurs in the reactive regions of a flame, it is a suitable indicator of the position of the flame. However, being a line-of-sight technique, collected images are averaged along the perspective line of the camera lens. In the present work, chemiluminescence imaging was used to visualize the position, size, and shape of the flame. Imaging was also performed at a high repetition rate in order to observe the flame dynamics.

2.3 Particle image velocimetry (PIV)

Investigation of the flow fields in turbulent premixed combustion is essential to understand the flame stabilization and propagation as well as the chemical reaction processes involved [28]. Particle image velocimetry (PIV) is a commonly used optical technique for velocity field measurement in both a gaseous and a liquid medium. It can be performed in combination with other optical planar measurement techniques for visualizing the simultaneous flow field and species distribution. In use of the PIV technique for determining the velocity field, the flow under investigation needs to be seeded with small particles (or droplets). The principle on which the technique is based relies on accurate measurement of the displacement of the particles which are imaged in small regions and of the time of the displacement. The determination of the displacement $d(x; t_1, t_2)$ of the seeded particles within a short time interval $\Delta t = t_2 - t_1$, i.e.

$$d(x; t_1, t_2) = \int_{t_1}^{t_2} v\{x(t), t\} dt \tag{2.15}$$

here $v\{x(t)\}$ is the velocity of the seeded particles.

For obtaining precise imaging of the particles, two thin laser sheets are produced from two laser pulses, using a lens system. Usually, the sheet thickness is 0.5-1 mm for two-dimensional (2D) PIV, and the duration of the pulses is approximately 10 ns. It is an adequate exposure time that enables the particles to be imaged without being blurred, even at high velocities. The time separation Δt between the laser pulses is selected on the basis of two considerations: first, it is sufficiently long for determining the displacement of the seeded particles between the images, and second, it is short enough to discard those particles that have out-of-plane velocity components and have already left the laser sheet during the period between the two exposures. The size of the seeding particles also needs to be sufficiently small (1-10 μm) so that they can follow the motion without any time lag. The Mie scattered light [29] from the seeding particles is recorded. The seeding density should be relatively high and preferably be uniform. The size of the interrogation windows determines the spatial resolution. For resolving small structures, the interrogation windows require not only being of small size but also containing a sufficient number of particles for the velocity to be accurately determined. For good results, the number of seeded particles within an interrogation window needs to be approximately fifteen [29].

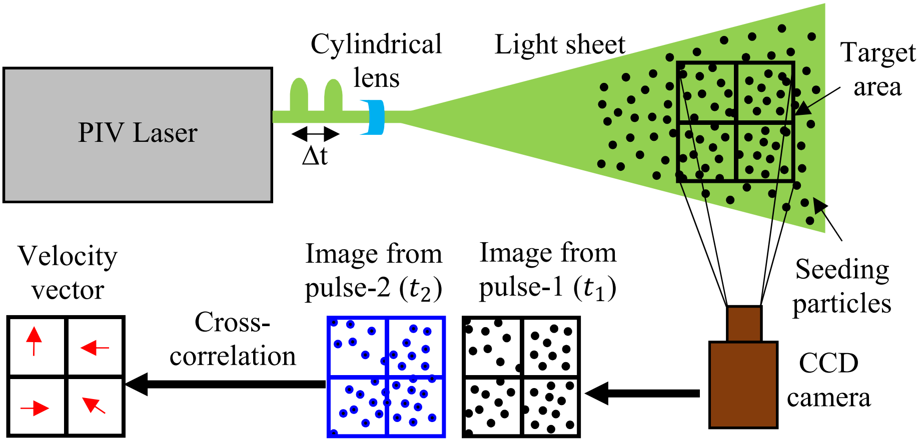

Figure 2.3: Basic principles of the PIV technique.

2.4 Emission measurement

The emission of combustion products was measured under different combustion operating conditions. Samples were collected using a water-cooled probe placed downstream of the combustion region at the end of the combustion chamber liner. In the experiments carried out, an Eco Physics model CLD-822Mhr nitrogen oxide (NO_X) detector, an MBE PAROX 1200 oxygen (O_2) detector, a Fuji ZKJ CO and CO_2 detector, and a JUM 3-300 un-burnt hydrocarbon detector were used.

Chapter 3

Equipment and data processing methods

In this chapter, section 3.1 presents a general description of different measurement equipment, in particular, different light sources and detectors that were employed in the experiments. In section 3.2, an overview of different post-processing tools that were employed for image analysis is provided.

3.1 Equipment

In section 3.1.1, various laser systems are described, followed by the description in section 3.1.2 of the detector systems.

3.1.1 Laser

In the thesis work, different diagnostic techniques were employed in the combustion studies, using the laser (Light Amplification by the Stimulated Emission of Radiation) as a light source. The laser emits monochromatic, directional and coherent light through a process termed stimulated emission of radiation and an amplification or increase of the intensity of the light. The stimulated emission allows a photon in a given mode to induce an atom or molecule that has an electron at an upper energy level to make a transition to a lower energy level and to emit a cloned photon into the same mode as the initial photon. These two photons, in turn, serve to stimulate the emission of two additional photons, as this process continues the properties of the photons being preserved. For stimulated emission to occur in an active medium, there need to be more atoms at the upper than at the lower energy level. This is known as a population inversion. The stimulated emission only occurs when the photon energy is equal to the atomic transition energy difference [30]. In a laser, an active medium that serves as an optical amplifier is placed in an optical resonator or cavity. The active medium can be a semiconductor, a crystalline solid, a gas or a liquid. In the simplest case, the cavity consists of two plane mirrors facing each other, surrounding the active medium of the laser. The one mirror has a high degree of reflectivity, whereas the other one is partially transmitting in order to allow the output to take place. The active medium can be stimulated to emit photons through external energy being applied using a flash lamp or another laser source. The selection of the wavelength, as an output, is achieved by choosing the active medium to be used and by selecting the dimensions of the resonator. Further refinement of the wavelength can be achieved by the inclusion of gratings or etalons in the resonator in order to favor a particular wavelength.

For a pulsed laser, the light and its optical power appear in a pulse of a particular duration at some repetition rate. Different techniques, such as Q-switching, mode-locking or pulsed pumping, can be used to produce light pulses of extremely high peak power as compared with those produced in continuous wave mode operations. In a Q-switched laser, the attenuator is placed inside the resonator to control the reflection of light between the two mirrors. When the attenuator is functioning, the photons that leave the gain medium do not return. Since a large population inversion can be built by limiting the stimulated emission radiation inside the cavity, no lasing occurs. It can also be defined as a reduction in the quality factor or 'Q' of the cavity. A low Q factor corresponds to high resonator losses per round trip and vice versa. When the Q factor is turned to high by removing the attenuator, an intense lasing builds up very rapidly for the high gain that takes place. It results in the generation of a highly intense lasing during a very short period of time [31]. The overall lasing process begins with a pumping of the gain medium, which excites electrons to a non-equilibrium state. A laser cannot function if there are only two energy levels for the absorption and emission processes. For such an atomic system, a population inversion cannot be achieved. For a system having two levels, the rate at which the upper level is populated through absorption equals that at which atoms leave through stimulated emission. The best it can do is at steady state or at saturation where no population difference remains between the lower and upper energy levels.

In a three-level system (Fig. 3.1), atoms or molecules are pumped from ground level (E_1) into the highest of the three energy levels, termed the pump level (E_3). From the pump level, spontaneous de-excitation occurs to an energy level (E_2) which is metastable. If the lifetime of the transition for $E_2 \rightarrow E_1$ is much longer than that of the transition $E_3 \rightarrow E_2$, the population of the excited state atoms or molecules accumulates at level E_2. The E_3 level then becomes unpopulated rather quickly. When over half the total population accumulates in the state E_2, a population inversion between level E_1 and level E_2 has been attained. However, a very strong pumping of the active medium is required in order to excite at least half of the population of atoms or molecules to obtain a population inversion. It is very challenging and makes three-level lasers rather inefficient. A four-level system has four energy levels instead of three and has the benefit of establishing no population inversion between the metastable (E_3) and ground electronic level (E_1). Instead, the population inversion there can be achieved between the metastable (E_3) and a lower-lying short-lived energy level (E_2). Only a few atoms or molecules are needed to be excited into the upper level to achieve a population inversion. A four-level laser is more effective than a three-level one, and most practical lasers are of this type [30].

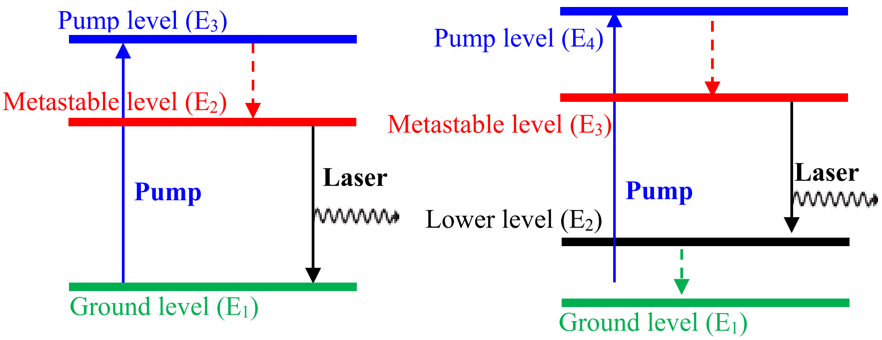

Figure 3.1: Energy level diagrams of different laser systems. The horizontal lines indicate energy levels; the higher a line is, the higher the corresponding energy is. Left: a three-level system, where the laser transition ends on the ground state. Right: a four-level system, where the laser transition ends on a level above the ground state, which is quickly depopulated, e.g., via phonons model.

3.1.1.1 Nd: YAG laser

The Nd: YAG laser is one of the most frequently employed high-power pulsed solid state lasers. It is a four-level system that uses a crystalline rod of neodymium-doped yttrium aluminum garnet crystal (Nd: $Y_3Al_5O_{12}$) as the gain medium. A large population inversion in the active medium is achieved by limiting the build-up of stimulated emission radiation inside the cavity and using the Q-switching technique. The fundamental output wavelength of the most widely used Nd: YAG laser is 1064 nm. This wavelength can be frequency doubled to 532 nm by use of a non-linear crystal. This process is called second harmonic generation and has an efficiency of approximately 40-50%. Higher harmonics, third (355 nm) and fourth (266 nm), can be obtained by introducing additional non-linear crystals. The laser radiation at 532 nm and 355 nm can be used to pump dye lasers to reach other wavelength regions.

The Nd: YAG can be used for different applications, such as for fuel visualization [32], formaldehyde visualization [33], laser-induced incandescence [34], and flow field measurement [35]. In the present work, different Nd: YAG lasers and their harmonics were employed for pumping the dye lasers as well as for fluorescence imaging of various combustion intermediate species. A second harmonic (532 nm) of the Quantel YG980 was used to pump a dye laser for OH-PLIF applications, whereas a Quantel Brilliant B was used for CH_2O-PLIF measurements. The Nd: YAG laser systems employed have a repetition rate of 10 Hz, and typically a ~ 10 ns pulse duration.

3.1.1.2 Dye laser

A dye laser utilizes organic dyes dissolved in liquid solutions as a lasing medium and is widely tunable, employing various dye solution. Organic dye molecules show both broad absorption and fluorescence spectra because of the complex structures of polyatomic dye molecules. Large molecules can emit a wide range of wavelengths due to the different vibrational-rotational energy states found within a given electronic state. Dye lasers are usually pumped optically by a flash lamp or by another laser. Frequency doubling or tripling can be achieved through the use of harmonic generation crystals to extend further the operational wavelength range of the dye laser.

In the thesis, a Continuum ND60 dye laser was used for the OH-PLIF application. A dye solution of Rhodamine 590 and methanol or ethanol was used to generate 576 nm. This wavelength was then frequency doubled using a KDP crystal to produce a 283 nm wavelength for the OH transitions scheme $A^2\Sigma^+(v'=1) \leftarrow X^2\Pi(v''=0)$. Dye lasers are prone to mode hopping, in which the wavelength changes from shot to shot [36]. Therefore, it can cause significant errors in quantitative measurements.

3.1.2 Detectors

For recording images or obtaining two-dimensional data, use of charged coupled devices (CCD) and complementary metal-oxide semiconductor device (CMOS) cameras is advantageous. Both these technologies use the same principle for photon capture, yet the signal is extracted from the individual pixels in different ways. Various investigations involving imaging were conducted within the framework of the thesis using both image-intensified CCD (ICCD) and CMOS cameras.

CCD (ICCD) camera

For imaging, the collected signals are focused onto a photocathode that converts the incoming photons to electrons. The electrons are then accelerated and amplified in a microchannel plate (MCP). The high voltage applied to the MCP forces the electrons to hit the walls of the channels and generate secondary electrons. An avalanche of electrons is created. Then the electron cloud hits a phosphor screen that converts the electrons to photons again. After that, the photons are transferred by either a fiber-coupling or a lens system onto the CCD-chip, where they are read out. The CCD acts as an integrating device, holding the image information in a matrix of separate pixels. Each pixel is formed on a semiconducting substrate having a p- and an n-layer, an insulating oxide layer and metal conductors on the surface. Once the array of pixels has been exposed for the same amount of time, charges are accumulated in pixels. The readout process is initiated by shifting the charges along one dimension of the array by varying the potentials that isolate neighboring pixels [37]. The last pixel in the array dumps its charge into an output amplifier that converts the charge into a measurable voltage. The ICCD camera is integrated with an intensifier. The configuration of the ICCD cameras enables an ultra-fast gating of a few nanoseconds and delivers high photon-sensitivity even in the ultraviolet (UV) region. The intensifier makes it possible to detect weak signals, due to the amplification stage present in the MCP. A short exposure time (in the nanosecond range) of the camera can effectively reduce background luminescence for applications in which nanosecond laser pulses are employed.

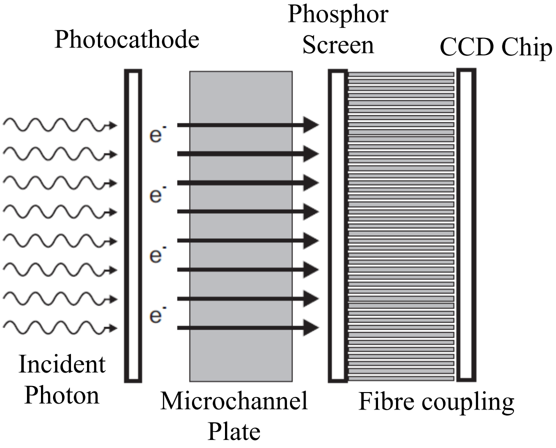

Figure 3.2: A schematic diagram of the basic principles of an ICCD camera.

CMOS

For the CMOS sensor, the readout time is much faster than the CCD imager. In CMOS technology, a readout is obtained from each pixel by column and row addressing and conversion of the charge to a voltage for each pixel. This procedure avoids the time-consuming readout process of the CCD imager. In this row and column addressing process, imaging can be restricted to areas of interest, with consequent gains in image collection speed. CMOS imaging systems are less frequently used in quantitative imaging since the pixel signal obtained can be less uniform than in the case of CCD imaging systems. However, this feature has been improved with the development of the CMOS active pixel sensor, which enables pixel amplification and correction of the pixel response [38].

3.1.3 Laser sheet optics

Both PIV and PLIF measurements were performed, using laser sheets that were formed by use of sheet-forming optics. For PLIF measurements, a collimated laser sheet was created by combining a -40 mm cylindrical lens and a positive +500 mm focal-length convex lens +50 mm in diameter. Both of the lenses were arranged with coincident foci, which generated a parallel sheet approximately 50 mm in width. With the use of the collimated laser sheet, beam alignment and beam profile correction became more straightforward and more accessible. For PIV measurements, a divergent laser sheet was used to cover the larger area for probing.

3.2 Data processing methods

It is always desirable to collect and generate an image or spectrum with a high signal-to-noise ratio (SNR). Digital image processing was performed on recorded images to improve the signal-to-noise ratio. Also, for analyzing the different properties of the combustion processes and the physical phenomena involved, various statistical or analytical treatments were implemented on the acquired data or image. These post-processing tools are employed with the use of Matlab and are described in this section.

3.2.1 Proper orthogonal decomposition (POD)

Proper orthogonal decomposition (POD) is an advantageous statistical method that can be used as a post-processing tool to decompose a given ensemble of signals into a spatial and a temporal part, the spatial part corresponding to the mode and the temporal part corresponding to the time evolution of the mode. This method is also known as the Karhunen-Loeve procedure, principal component analysis (PCA) and empirical component analysis [39]. It is widely used for better understanding the spatial and temporal behavior of the flow field. In the thesis, the POD is applied to high-speed chemiluminescence data to investigate the flame dynamics that would be lost with the use of classical time averaging statistics. The POD can complement the average field with relevant information regarding the most energetic modes of the flame dynamics [40]. The POD can decompose a given ensemble of data U (2D arrays in the present case) into a set of Eigenfunctions. It results in a certain number of orthogonal spatial Eigenfunctions or modes $\Psi_i(x)$ and time coefficient $g_i(t)$. Any instantaneous snapshot $U(x, t_f)$ taken at time t_f, can be reconstructed in terms of a basis of Eigenfunctions that represent the typical modes of the ensemble.

$$U(x, t_f) = g_0 \Psi_0(x) + \sum_{i=1}^{\infty} g_i(t_f)\, \Psi_i(x) \tag{3.1}$$

here, $\Psi_0(x)$ or mode 0 represents the mean field whereas the subsequent modes represent fluctuations and thus the dynamics involved. The empirical basis of the POD is expressed mathematically as the following quantity which is to be maximized [41, 42]:

$$\langle |(U, \Psi)|^2 \rangle \big/ \|\Psi\|^2 \tag{3.2}$$

In Eq. 3.2, the $\langle\, .\, \rangle$ denotes the time or ensemble average, (a, b) represents an inner product and $\|c\|$ the norm:

$$(a, b) = \int_{\Omega_x} a.b^*\, dx \;\; and \;\; \|c\| = (c, c) \tag{3.3}$$

where Ω_x is the domain of interest, in which $U(x)$ and $\Psi(x)$ are defined. The asterisk (*) represents complex conjugation. Maximization of the quantity in Eq. 3.2 reduces to an eigenvalue problem [41, 42]:

$$\int_{\Omega_x} \langle U(x,t)\, U(x',t)\rangle \Psi(x') dx' = \lambda\, \Psi(x) \tag{3.4}$$

The details of the theory are not dealt with here. For the derivations and the implementation of the POD, the reader is referred to [41-43]. The domain Ω_x is discretized into a certain number of discrete points M for practical applications, and the eigenvalue problem has a size MxM. Sirovich's *Method of snapshots* [39] is applied and Eq. 3.4 is reorganized into a lighter eigenvalue problem of size NxN, where N is the number of instantaneous samples or snapshots (typically, M >> N). The eigenvalue problem reads as follows:

$$\begin{Bmatrix} b_{11} & \cdots & b_{1N} \\ \vdots & \ddots & \vdots \\ b_{1N} & \dots & b_{NN} \end{Bmatrix} \begin{Bmatrix} c_1 \\ \vdots \\ c_N \end{Bmatrix} = \lambda \begin{Bmatrix} c_1 \\ \vdots \\ c_N \end{Bmatrix} \tag{3.5}$$

where

$$b_{rt} = \int_{\Omega_x} U(x,t_r).\, U(x,t_p)\, dx \tag{3.6}$$

For the eigenvalue problem, N number of eigenvalues λ_i can be obtained as a result. Each of the eigenvalues λ_i corresponds to a mode $\Psi_i(x)$ and N eigenvectors $c_i(t_f)$. In the method of snapshots, the modes are expressed as a linear combination of the following instantaneous realizations:

$$\Psi_i(x) = \frac{1}{\lambda_i N} \sum_{f=1}^{N} c_i(t_f) U(x,t_f) \tag{3.7}$$

The eigenvalues are ordered in descending order $\lambda_i > \lambda_{i+1}$ and represent the energetic content of the modes. Therefore, in implementing the decomposion on the ensemble of data U, the first POD mode is found to be the highest energetic and typically identifies coherent structures. The time coefficients in Eq. 3.1 are computed by projecting the modes on the snapshots. The time coefficient relative to the i-th mode and the f-th instantaneous sample reads as follows:

$$g_i(t_f) = \Psi_i(x) \times U(x,t_f) \tag{3.8}$$

3.2.2 Deconvolution of the chemiluminescence image

In combustion research, many non-intrusive optical techniques, such as IR emission for flame temperature measurement and chemiluminescence imaging, are used that provide line-of-sight projections of a flame field [44, 45]. Abel's integral equation can play an essential role in such cases, where the radial distribution of any quantity of the axisymmetric flame is acquired from the projections of the flame. The deconvolution of the projections can be used to reconstruct the spatial field of the measured properties at the symmetry plane through the center of the flame. In this work, the time-averaged chemiluminescence flame images are deconvoluted applying the Onion-peeling method.

3.2.2.1 Onion-peeling method

It is assumed here that the line-of-sight integrated projection data are taken at evenly spaced radial locations from an experiment. A cylindrically symmetrical field distribution $F(r)$ and line-of-sight integral projection data $P(x)$ are shown in Fig. 3.3, as given by

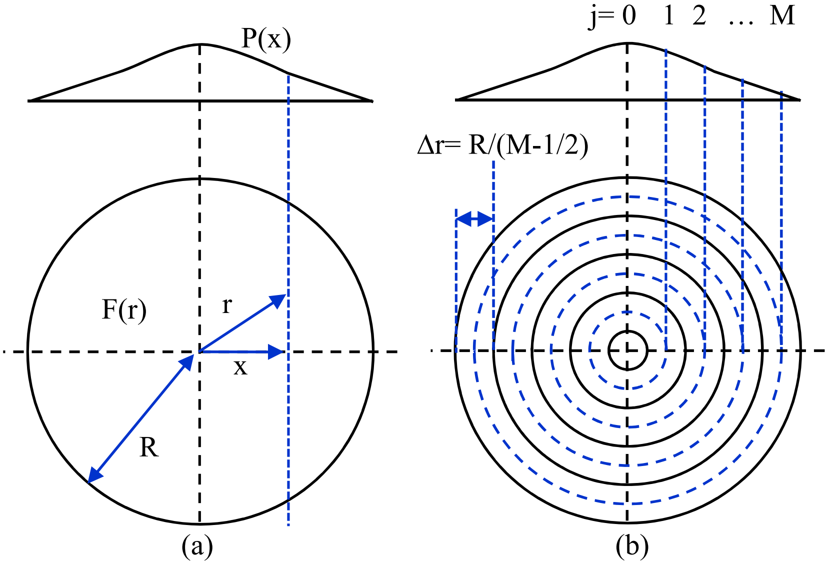

Figure 3.3: a) A cylindrically symmetrical field distribution F(r) and line-of-sight integral projection data P(x) are shown, and b) discretization of the problem domain.

$$P(x) = \ 2\int_{x}^{R} \frac{F(r)}{(r^2 - x^2)^{1/2}} dr \tag{3.9}$$

This is a form of Abel's integral equation [46]. In the generic form of Abel's equation, $F(r)$ is referred to as the field variable, and $P(x)$ is the projected data. The analytic inversion of the projection data to provide the field $F(r)$ is the well-known Abel transform,

$$F(r) = \frac{-1}{\pi}\int_{x}^{R} \frac{P'(x)}{(x^2 - r^2)^{1/2}} dy \tag{3.10}$$

where $P'(x) = \ dP(x)/dx$. However, this solution is rarely used in practice since it requires the derivative of the projection data which is usually unknown and approximating $P'(x)$ by use of a finite-difference scheme increases the experimental error present in the $P(x)$ measurements [46]. This effect is also aggravated by increasing the number of projections and limiting the resolution of $F(r)$. In contrast, having a quite less number of $P(x)$ values to estimate $P'(x)$ can lead to large errors in $F(r)$, due to truncation of the higher-order Taylor series terms. There is a diverse set of numerical techniques for solving Abel's equation. The onion-peeling method is one of the simplest and most commonly used methods for solving Abel's equation [47], a method in which the measured field is divided into M evenly spaced annular elements of thickness $\Delta r = R/(M - 1/2)$, as shown in Fig. 3.3(b). If $F(r)$ is assumed to be uniform over each element, Eq. 3.9 is transformed into

$$P_i = 2\sum_{j=i}^{M-1} F_j \int_{\substack{r_i, j=i \\ r_j - \frac{\Delta r}{2}, j>i}}^{r_j + \frac{\Delta r}{2}} \frac{r}{\sqrt{r^2 - x_i^{2}{}^{2}}} dr \tag{3.11}$$

where, $x_i = i\Delta r, r_i = j\Delta r, P_i = P(x_i)$ and F_j approximates $F(r_j)$. The projected data are thus as shown in Eq. 3.11

$$P(x_i) = \sum_{j=i}^{M-1} A_{op,ij} \,.\, F(r_j) \tag{3.12}$$

For each annular element, Eq. 3.12 gives rise to a set of linear equations that can be rewritten as $A_{op}w = b$, where $\boldsymbol{w}$ contains the unknown field variables, $w^T = \{F_i, i = 0,1 \dots \dots, M - 1\}, b$ contains the projected data set, $b^T = \{P(r_i), i = 0,1 \dots \dots, M - 1\}$, and

$$A_{op,ij} = \begin{cases} \mathbf{0} & \boldsymbol{j < i} \\ 2\Delta r \, \{(j + 1/2)^2 - i^2\}^{1/2} & \boldsymbol{j = i} \\ 2\Delta r \, \{(j + 1/2)^2 - i^2\}^{1/2} - \{(j - 1/2)^2 - i^2\}^{1/2} & \boldsymbol{j > i} \end{cases} \quad (3.13)$$

The element $A_{OP,ij}$ represents the contribution of $F(r_j)$ to the projected variable $P(x_i)$ and is equal to the length of the chord passing through x_i that lies within the jth annular element. Since A_{op} is an upper triangular matrix, w is readily solved for by back substitution.

3.2.3 Edge detection of OH-PLIF image

Using OH-PLIF images to locate the transient reaction zones in highly turbulent flame is not always straightforward since the detectable amount of OH exists in abundance, not only in the reaction zone but also in the burned gases, where the temperature of the gases is approximately above 1400 K. However, the equilibrium OH concentration increases exponentially with temperature. Thus, in the reaction zone where the temperature is at a maximum, one can expect a sharp temperature gradient and a correspondingly sharp OH-PLIF intensity gradient. The strong temperature gradients together with the existence of a super-equilibrium OH concentration in the reaction zone results in sharp gradients being found in the OH-PLIF images [35, 48]. Thus by deducing the gradients of the OH-PLIF distributions in the axial and radial directions, the spatial location and the structure of the transient reactions zones can be identified. Before extracting the flame-front edge, median and Gaussian filters are applied to the OH-PLIF images for smoothing the images and reducing the high-frequency noise content of the original OH-PLIF image. These filtering processes also reduce the number of erroneous curves that may be detected later by the gradient or derivative operation and improve the accuracy of the flame-front detection. The first derivative, both in the x- and y-direction, can be calculated by convoluting the original images with two kernels. One is for calculating the changes along the horizontal axis, and the other is for calculating those along the vertical axis. The size of the kernels can be 2 x 2 or 3 x 3. The sharp gradients are found in the flame front, whereas the weaker gradients correspond to the boundary layers between the hot and the cold gases. These weaker gradients have been masked out by use of a threshold that is 20% of the maximum gradient value.

3.2.4 Probability density map (PDM)

For calculating the probability density mapping (PDM) of the PLIF or chemiluminescence single-shot images, the images were processed by assigning a value of 1 to areas containing a signal and of 0 to regions containing no signal, to prepare binary images of the signal distributions. Those binary images were then accumulated and normalized. For PLIF applications, the probability density mapping of single-shot images is advantageous since it shows the spatial distribution of the signal which is not affected by the laser power fluctuations of the excitation wavelength.

Chapter 4

Gas turbine related combustors

A gas turbine is a combustion engine which converts fuel to mechanical power. Gas turbines are used mainly for electric power production and for aircraft jet propulsion. Almost all of the combustion devices that are investigated in the thesis are related to the gas turbine. This chapter provides an overview of the various combustion devices that are studied in the thesis.

4.1 Gas turbine

A gas turbine consists of three primary sections: a compressor, a combustor, and a turbine. The compressor and turbine are mounted on the same shaft. Inside the compressor, the air is compressed to a high pressure and then enters the combustor (or combustion system), where it is mixed with fuel, resulting in combustion. The produced hot exhaust gases expand through the turbine section, where part of the energy is used to drive the compressor mechanically, and the rest can be used for various other purposes, such as for generating electricity in the case of a land-based gas turbine and for producing thrust in the case of a jet aircraft. The Brayton cycle explains the thermodynamic process taking place in gas turbines. The cycle consists of four steps, as shown in Fig. 4.1. P-V and T-S diagrams present the changes in the thermodynamic properties of the working fluid. The ambient air is compressed isentropically (in the ideal case) in the compressor section. Therefore, the pressure and temperature of the air increase in the step from state 1 to state 2. In the next stage inside the combustor from state 2 to state 3, heat is added at constant pressure for fuel-air combustion. The high-temperature gas is then expanded isentropically in the turbine section from state 3 to state 4 through the conversion of kinetic energy to mechanical energy. For a closed gas turbine cycle, the exhaust gas can be cooled (heat loss at constant pressure) and be recirculated at that stage from state 4 to state 1 [49]. Since without the addition of heat the cycle cannot be operated, the combustion system itself is an essential part of gas turbine operations.

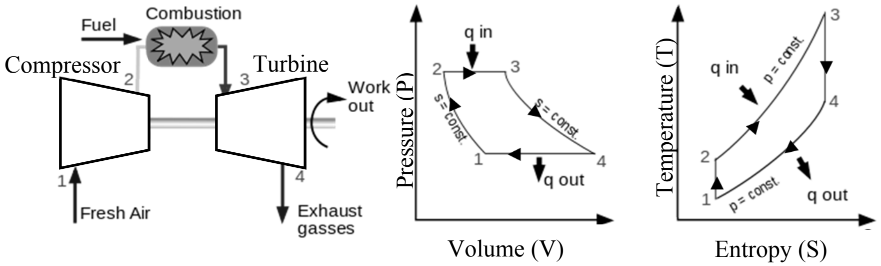

Figure 4.1: A gas turbine cycle and its components according to [49]. A pressure (P) vs. volume (v) diagram and a temperature (T) vs. entropy (s) diagram for the Brayton cycle. 'q' represents the addition and subtraction of heat.

In the field of gas turbine system development, it is imperative to minimize pollutant emissions in order to be able to maintain a clean environment and meet existing legislative mandates [50]. Although, the non-premixed operation of a gas turbine combustor provides more stable and easily controllable combustion than premixed operation does; it has drawbacks regarding pollutant emission levels. Non-premixed combustion occurs under close to stoichiometric condition and produces high NO_X emission levels because of the high flame temperatures. Moreover, the presence of fuel-pockets in the hot regions can lead to increased soot formation. For reducing NO_X production, the approach of lean premixed combustion is already a recognized technique in the field of stationary gas turbines. It provides lower combustion temperature and limits the thermal NO_X production pathways [3, 4]. However, the lean premixed mode of operation may lead combustion towards unstable conditions that induce local extinction, poor combustion efficiency, and combustion instabilities [5]. The inclusion of a diffusion pilot flame and a pre-chamber combustor in burner design can help to stabilize the lean premixed combustion [6] and ensure lower NO_X emissions [7].

4.2 Emissions

The exhaust gases from a gas turbine are composed of carbon monoxide (CO), carbon dioxide (CO_2), water vapor (H_2O), unburned hydrocarbons (UHC), and nitrogen oxide (NO_X) for using hydrocarbon fuels. Among these, carbon dioxide (CO_2) and water (H_2O) are inevitable products of combustion. However, CO_2 can be can also be regarded as a pollutant, since it contributes to global warming and its production can only be reduced by burning less fuel. CO is toxic, and it reduces the capacity of the blood to absorb oxygen and at high concentrations, can cause asphyxiation and even death. Some unburned hydrocarbon can be toxic depending on the species, and also these may combine with oxides of nitrogen to create photochemical smog [5]. In addition, oxides of nitrogen (NO + NO_2) can cause acid rain. NO_X is created mainly from the combustion air at high flame temperatures. If combustion does not include any fuel containing nitrogen, nitrogen oxide (NO_X) is formed by four chemical mechanisms or routes that involve nitrogen from the air: the thermal or Zeldovich mechanism, the Fenimore or prompt mechanism, the N_2O-intermediate mechanism and the NNH mechanism [2].

Zeldovich mechanism

The primary route for the production of NO_X is via the thermal mechanism described by Zeldovich [2, 51], which is dominant in high-temperature combustion over a wide range of equivalence ratios. The rate of formation of NO_X is high above around 1900 K, as shown in Fig. 4.2.

The Prompt mechanism

In the prompt mechanism, NO_X is formed more quickly than predicted by the Zeldovich mechanism [52]. NO_X is produced by following either the CN or the HCN reaction pathway. The general scheme of the mechanism is that hydrocarbon radical react with molecular nitrogen to form amines or cyano compounds. Then the amines and the cyano compounds are converted to intermediate compounds that ultimately form NO. In this mechanism, NO is produced in the flame region very early, and it appears at all temperatures.

The N_2O-intermediate and NNH mechanisms

The N_2O-intermediate mechanism can be a significant contributor to NO_X emissions under lean conditions in which the temperature is low, and the level of thermal NO_X formation is low as well. Besides, the NNH mechanism plays a vital role in the NO formation that takes place in the combustion of hydrogen and hydrocarbon fuels having large carbon-to-hydrogen ratios [53].

Some fuels contain nitrogen in their molecular structure. The fuel-bound nitrogen can also be converted to NO_X and can add one more NO formation pathways to those already discussed. Biofuels produce higher amounts of fuel

NO_X than gaseous fuels do. In the combustion of fuels containing bound nitrogen, the nitrogen is rapidly converted to hydrogen cyanide (HCN) or ammonia (NH_3), and then they follow the prompt mechanism. The most effective way of minimizing NO_X production is to reduce the maximum temperature in the combustion zone. This can be achieved for both fuel-rich and fuel-lean combustion since the flame temperature is low in both cases. In contrast, the production of carbon monoxide (CO) increases at the low flame temperature as shown in Fig. 4.2 [5]. CO is formed when the fuel does not receive sufficient oxygen to complete the reactions taking place under fuel-rich conditions. Under fuel-lean conditions, CO can also be formed if the flame temperature is sufficiently low to slow down the rate of oxidation of CO to CO_2. The emission of CO increases at temperatures above 1900 K since above this temperature the dissociation of CO_2 to CO becomes significant. Minumum levels of emission of both CO and NO_X can only be achieved within a narrow range of flame temperatures (as shown in Fig. 4.2), since the production of CO increases below flame temperatures around 1650 K, and the production of NO_X rises above temperatures around 1900 K. Consequently, it is imperative to design a gas turbine combustor in such a way that the flame temperatures remain within this interval [5].

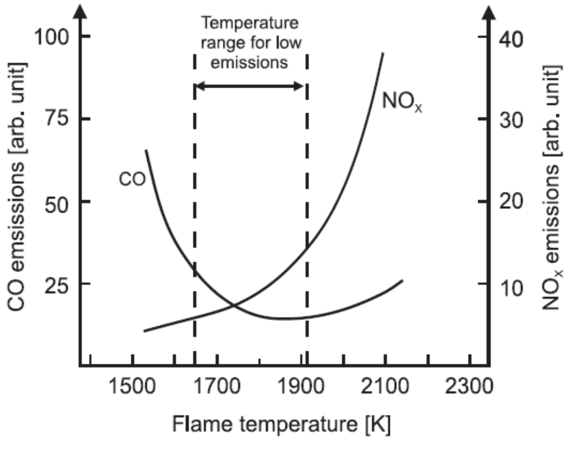

Figure 4.2: A diagram showing the effects of the flame temperature on CO and NO_X *emissions. The production of thermal* NO_X *increases with temperature and higher amounts of CO is produced at temperatures below 1650 K. Minimum emissions of CO and* NO_X *can only be achieved within a narrow range of temperatures [5].*

4.3 The flame

In a modern gas turbine combustion system, it is mainly the premixed flame that can be observed. However, part of the processes can also involve non-premixed (diffusion) flames or partially premixed flames. The lean premixed approach to combustion is an established technique for obtaining low NO_X emissions since the temperature of a lean premixed flame is lower than that of a diffusion flame [54]. However, the lean flame is more prone to become unstable, and thus diffusion pilot flames are still used to improve the flame stability under lean operating conditions.

Laminar premixed flames are well described in [55-57]. In a premixed flame, the fuel and oxidizer are perfectly mixed before combustion. The equivalence ratio (ϕ), which quantifies the fuel to oxidizer ratio, can be expressed as

$$\phi = \frac{m_{fuel}/m_{oxidizer}}{\left(m_{fuel}/m_{oxidizer}\right)_{st}} \tag{4.1}$$

where m_i refers to the mass of the i component in the mixture. The overall structure of a planar freely propagating CH_4/air stoichiometric laminar flame, a one-dimensional flame, is shown in Fig. 4.3 [58]. The main features of the structure are three different zones: the preheat zone, the inner layer or reaction zone and the oxidation zone. In the reaction zone or inner layer, which has a thickness of less than 1mm, most of the chemical reactions occur [58]. Far upstream of the flame, the temperature of the fuel and air mixture is defined by the intel temperature, whereas it increases rapidly and monotonically in the preheating zone and the reaction zone. In the preheating layer, the reactants are preheated with the heat that is diffused and conducted from the reaction zone. However, only a limited number of reactions occur, since the temperature is lower than the cross-over ignition temperature, and so the reactive radicals are quickly consumed. At the inner layer or reaction zone, the temperature becomes higher than the cross-over ignition temperature (about 1000 K), due to the domination there of chain-branching reactions over chain terminating reactions. This also accelerates the overall combustion reaction process. At the starting of the thin reaction zone, the fuel begins to decompose with the formation of CH_2O. Then, CH_2O and other intermediate reactants are quickly consumed as soon as the production of such reactive radicals like OH accelerates the reactions. The peak of the heat release rate is located at the center of the reaction zone. The temperature and major combustion products (such as CO_2) increase rapidly and monotonically at the end of the preheat zone and in the reaction zone. In the oxidation layer, chemical reactions can occur since the temperature is still high there. As a result, the OH radical concentrations and the continuous growth of NO can be observed. However, most of the chemical reactions in this zone reach equilibrium. This zone is also known as the post-flame zone. There, both the combustion product distributions and the temperature are rather flat and the heat release rate is not significant.

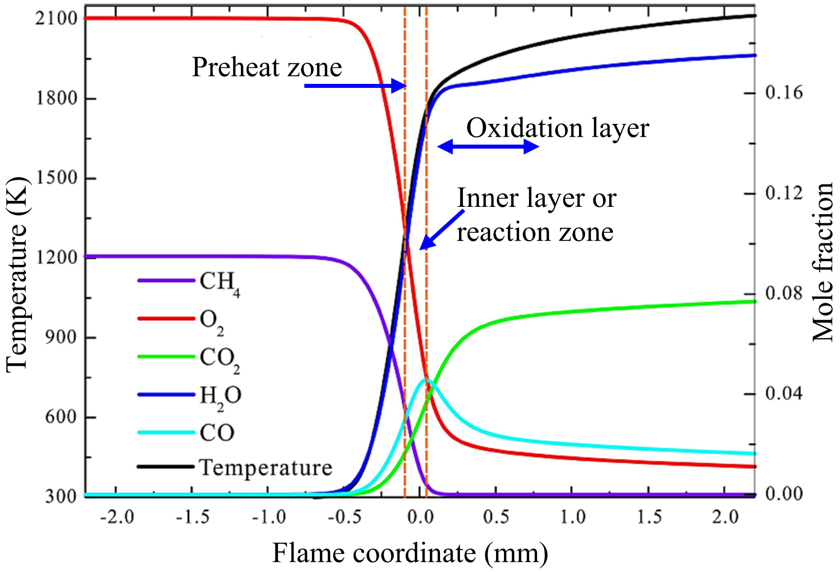

Figure 4.3: The overall structure of a planar freely propagating methane/air stoichiometric flame is shown here in accordance with [58].

4.4 Flame-turbulence interactions

Turbulence is a random process. Due to turbulence-flame interactions, the laminar premixed flame structure can change abruptly. In this process, the velocity and various scalar quantities, such as the flow velocity, species concentrations, and temperature, fluctuate randomly. The variations in temperature generate changes in the chemical reaction rates, leading to the laminar flame front becoming wrinkled and fluctuating. In a gas turbine, a turbulent flame is favorable since it accelerates the combustion process by enhancing the transfer process of heat, mass, and momentum. The size of the flame and the combustor can be reduced while maintaining the same load and power output as before. The Reynolds number (Re) is a very useful dimensionless quantity. It is used for predicting the transition from laminar to turbulent flow, and for the scaling of similar but different-sized flow situations. The Reynolds number [59] is defined as

$$Re = \frac{\rho u L}{\mu} = \frac{uL}{v}; \tag{4.2}$$

here, ρ is the density of the fluid, u is the velocity of the fluid, L is a characteristic linear dimension, μ is the dynamic viscosity of the fluid, and $v = \mu/\rho$ is the kinematic viscosity of the fluid.

Turbulence is composed of eddies of different sizes. Large eddies are unstable. They tend to break up into smaller ones by transferring their energy to smaller ones. The largest eddies, integral scale, have a length scale l_0, velocity $u' \equiv u(l_0)$, and time scale $\tau_0 = l_0/u'$. The smallest eddy is the Kolmogorov eddy, and its length, velocity as well as time scale are η, $u_\eta \equiv u(\eta)$, $\tau_\eta = \eta/u_\eta$ respectively. In addition to the flow scales, for a given mixture of fuel and air there are two important scales: the laminar flame speed (S_L) and and the laminar flame thickness(δ_L). The term $\tau_c = \delta_L/S_L$ is the chemical time scale during which a premixed flame propagates a distance of the flame thickness. It also indicate the time during which a product is formed. For characterizing turbulent premixed flames, the Damköhler number (Da) and the Karlovitz number (Ka) are also commonly used as non-dimensional numbers. These numbers quantify the extent of the turbulence/chemistry interaction. Ka is defined as the ratio of the chemical time scale, τ_c to the Kolmogorov time scale, τ_η, whereas Da is the ratio of the integral time scale τ_o to τ_c [60]. Mathematically,

$$Ka \equiv \frac{\tau_c}{\tau_\eta} = \frac{\delta_L u_\eta}{\eta S_L} \tag{4.3}$$

$$Da = \frac{\tau_o}{\tau_c} = \frac{l_o S_L}{\delta_L u'} \tag{4.4}$$

For $Ka \leq 1$, the flame propagation time is shorter than the smallest turbulent eddy time scale and the flame is thinner than the smallest eddies scale. For $Da \geq 1$, the length scale of the largest eddies is typically much larger than the laminar flame thickness.

A diagram using the velocity (u'/S_L) and the length scale (l_0/δ_L) ratios to classify different regimes of premixed turbulent combustion was proposed by Borghi [61] and was later modified by Peters [55]. Here, S_L is the laminar flame speed, δ_L is the laminar flame thickness, l_0 is the integral length scale of turbulence, and $u'$is the RMS velocity, which represents the turbulent kinetic energy. The ratio u'/S_L also indicates the degree of turbulent intensity. In the regime diagram, according to Peters [55], the thin reaction zone is the regime as defined by $1 < Ka < 100$. In this regime, turbulent scales are small, and the flame front can be expected to be distorted by turbulence. The Kolmogorov eddies can enter into the preheating zone but cannot penetrate into the inner layer or the reaction zone. This regime is also called the thickened-wrinkled flame [60]. The burner, investigated in papers II, III, IV, and V had a testing range within the thin reaction zone. This diagram can provide useful directions, but the regime demarcation is based entirely on qualitative analysis. Therefore, it cannot be considered as providing precise guidance, and the reasons are explained in [62].

4.5 Swirl flame stabilization

In a gas turbine combustion system, both the flame-anchoring position in the combustor and flame stabilization play a vital role, since any aberration from the desired flame location, along with instabilities of the flame, may not only affect the combustor life due to high thermal stress but also cause unwanted emissions. Various approaches, such as pilot flame stabilization, use of a bluff body, and swirl stabilization, can be used for flame stabilization in different applications [60]. In a gas turbine for lean premixed flames, the swirl stabilization is a widely accepted process. At sufficiently high levels of swirl, a flame is stabilized forming a central recirculation zone (CRZ) downstream of the burner nozzle [63, 64]. Swirling flow generates a natural radial pressure gradient caused by axial decay of the tangential velocity. The incoming (swirling) jet flow of the air-fuel mixture expands in a radial direction, an adverse pressure gradient being created in the centreline. A recirculation of the flow occurs in the center, a CRZ being formed. The CRZ helps flame stabilization by a two-fold mechanism. First, this process increases the residence time of the mixture in the combustion chamber through reducing the axial velocity. Secondly, it brings the hot product gases that can re-ignite the possibly quenched flame and preheat the incoming air-fuel mixture [64]. Together with a CRZ, outer recirculation zones (ORZs) can also be formed through sudden expansion of the flow in a radial direction. For flame stabilization, it is necessary to avoid flashback and lean blowout. The local flame speed needs to be lower than the velocity of the approaching flow to prevent flashback, but it should not be too low since the flame can then move downstream to cause a lift-off or a blowout.

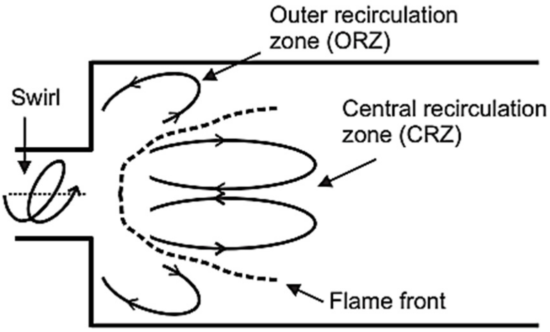

Figure 4.4: Flame stabilization by swirl [15].

4.6 The gas turbine combustion system

The combustion system is one the most critical parts of a gas turbine since its task is to convert chemical energy to heat and increase the temperature of the flow before the turbine. A good combustion system can ensure proper fuel-air mixing, adequate flame stability, significant dilution, and an essential temperature match at the exit profile. The combustor system consists mainly of the burner or nozzle section and the combustor. The mixing of fuel and air is accomplished in the burner or nozzle section, whereas the fuel-air mixture is burned inside the combustor. Maximum combustion efficiencies, minimum emissions, fuel flexibilities, and capabilities of reliable operations avoiding instabilities, lean blowout, auto ignition as well as flashback are highly important features to take account of in designing a nozzle/burner system [65]. There are different ways of arranging the combustors in a gas turbine. In an annular combustor, many burners share a single large combustion chamber, whereas many numbers of can type combustors can be placed in an annular arrangement with their burners [66]. All combustors share certain common design rules to achieve efficient and stable combustion. A diagram of a generic gas turbine combustor is shown in Fig. 4.5. Combustion is initiated in the primary zone, the flame being anchored and stabilized there. Cooling air is provided at various locations within the combustor to protect the surfaces involved from excessive temperatures [67]. At the combustor exit, dilution air is added to create and maintain an appropriate temperature distribution, as determined by the desired turbine inlet temperature.

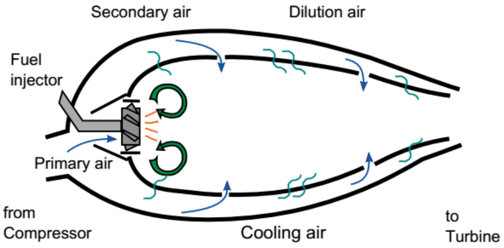

Figure 4.5: General layout of a gas turbine combustion chamber [67].

4.6.1 The 4th generation dry low emission (DLE) burner

In the thesis, the majority of the work involves different investigations that were performed on a downscaled prototype 4th generation dry low emission (DLE) burner. Siemens Industrial Turbomachinery designed this burner and the studies carried out concerns the development of the SGT-750 DLE burner. A survey of the history of the development of the DLE burner and the principles that are involved is to be found in ref [68]. The burner assembly is composed of three concentrically arranged sectors: a radial swirled outer sector (Main), an axial swirled intermediate sector (Pilot), and a central-body burner or RPL (Rich-Pilot-Lean) section. In the tested prototype burner, the Pilot and the Main sections are scaled down to one-third (1/3) from the SGT-750 burner, whereas the RPL is kept at the same scale. The cross-section of the burner assembly in full configuration is shown in Fig. 4.6. The fuel flow to each of these sections is regulated independently, and the central body RPL having separate fuel and air feeds. The ability to vary the equivalence ratios of the three sections enables the burner to achieve optimized combustion. For reducing NO_X production, the burner is operated by use of a lean premixed approach. The RPL produces heat and chemically active species or radicals to stabilize the flame. It can be operated from fuel lean to fuel rich conditions, and the selection of leaner or richer conditions depends on two considerations: a) optimization of the combustion stability near lean blowout limits [9] and b) minimization of NO_X production [50]. The increase in the equivalence ratio of RPL improves the lean blowout limit [9]. As a side effect, it also increases the NO_X production [50]. The RPL burner has a mixing chamber in which fuel and air enter tangentially and mix there. The intermediate section, the Pilot, helps to hold and stabilize the flame. In the Pilot, the fuel and air are partially premixed, since the short distance between the fuel injectors in the Pilot and the RPL-Pilot mixing tube (Fig. 4.6) limits proper fuel-air mixing there. The bulk combustion occurs in the outermost section, termed the Main. In the Main section, the fuel has a longer residence time and distance in which mixing can occur, since the fuel has been added sufficiently far upstream. The mixing takes place through the action of tangentially placed swirling vanes and intermediately positioned fuel injectors.

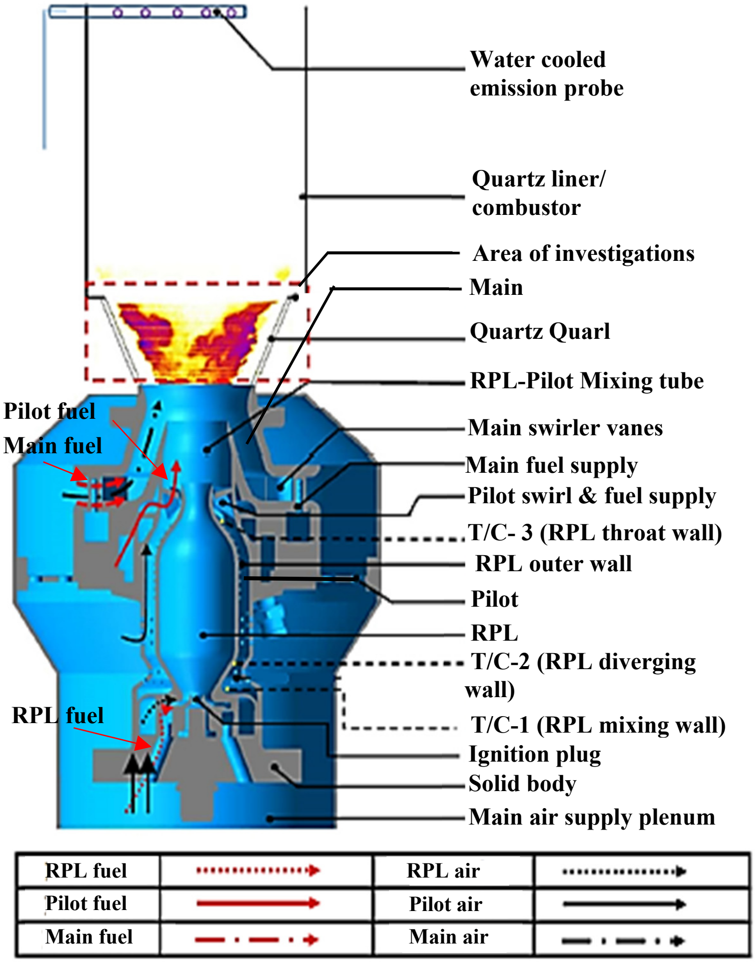

Figure 4.6: Cross-section of the prototype 4th generation DLE burner assembly.

The burner was installed vertically in a plenum in an atmospheric combustion test rig at Lund University. The same air plenum was used to supply the air mass flow required for both the Main and Pilot stages. The calculated air flow distribution using the effective areas was 21% through the Pilot and 79% through the Main burner pathway. On the basis of the calculated Pilot and Main air split, the fuel was injected into each section to maintain the same equivalence ratio (ϕ) in both the Pilot section and the Main section. The Pilot air stream entered the annular passage surrounding the RPL combustor through a series of holes. While passing through the annular passage, the pilot air picked up heat from the RPL combustor. All the fluid streaming from the respective burner sections were merged at the burner throat. At the burner exit, there was a diverging section, termed the Quarl, for smoothing both the flow and flame. It was made of quartz. It also enabled the flame stabilization zone to be visualized. A quartz liner 40 cm in length and 110 cm square in cross-section was mounted atop the burner assembly. At the end of the liner, combustion emissions were sampled using a water-cooled probe. A spark plug ignitor for initiating the combustion process was placed at the bottom center of the RPL. Three N-type T/Cs were placed along the outer wall of the RPL combustor: T/C-1 near the mixing chamber of the RPL, T/C-2 near the diverging section and T/C-3 at the site of the RPL throat/exit.

A similar prototype 4th generation DLE burner (version 1) was investigated for studying the flame and the emissions for varying fuel composition at atmospheric and elevated pressures conditions [9, 50, 69]. In the new test burner (version 2) hardware, certain modifications had taken place. In the version 1 burner, the Quarl was made of metal, and the scope for visualization of the flame inside the Quarl was limited. It was undesirable. Since the main flame of the burner is anchored at the Quarl, and the visualization of it is essential for understanding flame behavior at different operating conditions. In the version 2 burner, the metal Quarl had been replaced by a quartz one for enabling flame investigations to be carried out. In addition, downstream of the RPL and at the Pilot exit, a short passage distance, termed the RPL-Pilot mixing tube, was added to provide better mixing.

4.6.2 The TARS burner

The Triple Annular Research Swirler (TARS) burner is a laboratory-scaled generic burner that can simulate the characteristics of a gas turbine burner, regarding both the fuel injection and flame stabilization. It was developed by Delevan Gas Turbine Products in collaboration with General Electric Aircraft Engines. The TARS features three concentric interchangeable swirlers: two axial inner swirlers and a radially outer one (see Fig. 4.7). Different configurations can be obtained by changing the swirlers’ vane angles and their rotation directions. In the current investigations, the configuration to use was selected by removing the innermost swirler. The middle and outer swirlers co-rotate at vane angles of 45 degrees. The center of the burner is an open tube 10 mm in diameter, a strong central non-swirling jet being formed by removing the inner swirler. The TARS burner has a total length of 66 mm, the outer swirler having a diameter of

50.8 mm. In between the outer and middle swirlers, fuel injection holes are located to supply fuel for creating a pilot flame. However, in the current setup, these fuel injectors were not used since only premixed conditions were studied.

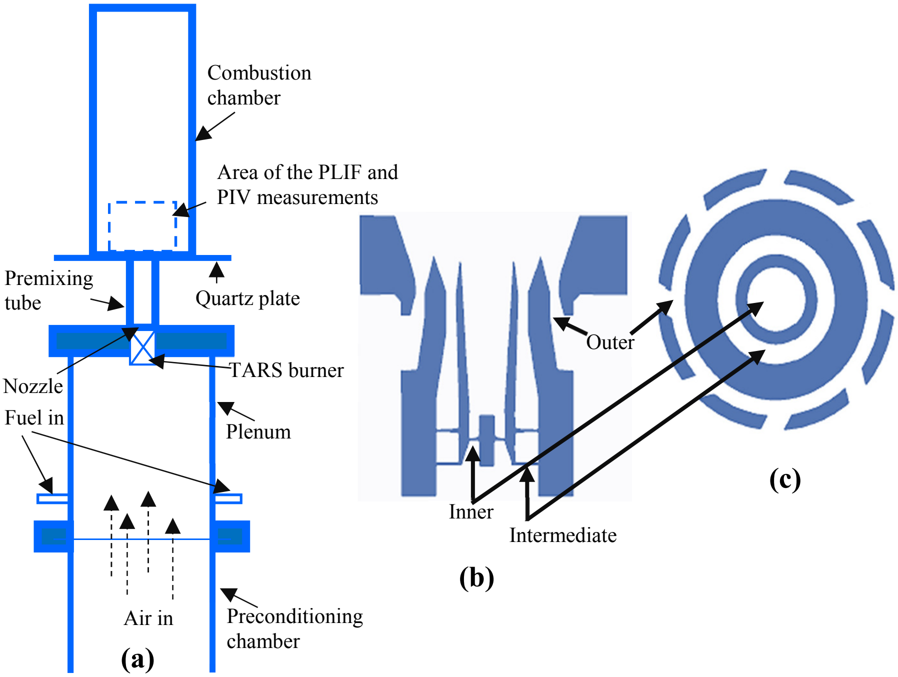

Figure 4.7: a) Cross-section of the TARS burner assembly, b) a longitudinal cross section of the TARS burner c) a perpendicular cross section of the TARS burner.

The burner was mounted vertically in the plenum of an atmospheric test rig in Lund. There was a flow conditioning chamber just before the plenum. A premixing tube 100 mm in length and having an inner diameter of 49.2 mm was placed at the exit of the burner. Three 400 mm long open-ended quartz combustion chambers were used for the investigations. The basic configuration had a 100 x100 mm square cross-section, whereas the two other combustion chambers had circular cross-sections with diameters of 101.6 mm and 128 mm, respectively. The premixing tube and the combustion chambers were made of quartz to provide optical access. The air flow passed through the flow-conditioning chamber to create a uniform velocity distribution before entering the plenum. Under premixed conditions, the fuel was injected at a considerable distance upstream of the base of the burner, in the plenum. An almost complete mixing of air and fuel had been achieved before the mixture entered the burner. For further details regarding the TARS burner, the reader is referred to ref. [40].

4.6.3 The CECOST laboratory-scale swirl burner

A laboratory-scale swirl burner was developed at Lund University based on the design concept of a modern gas turbine burner, and investigations were performed on this burner to study flashback and instabilities [70]. The burner, the design of which was inspired by the DLE burner, can simulate the complex turbulence-flame interactions. The swirl generator of the burner itself consists of four quarter-cones that are shifted with respect to each other to create a swirling flow. The flow enters the swirl generator in a combined tangential/axial/radial direction to create a swirling of the air. The cross-section of the burner assembly is shown in Fig. 4.8.

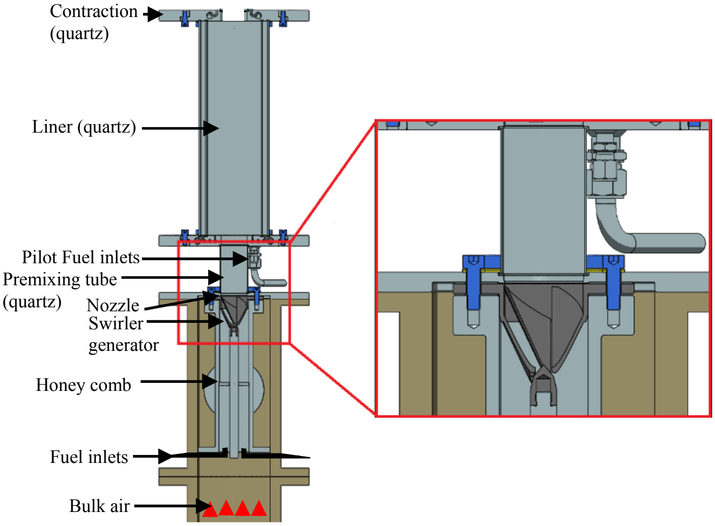

Figure 4.8: Cross-section of the CECOST swirl burner assembly.

The burner was installed vertically in a plenum in the atmospheric combustion test rig at Lund University. A cylindrical mixing tube 50 mm in diameter and 100 mm in length was placed downstream of the swirl generator. A liner or combustion chamber 400 mm in length and 100 mm square in cross-section was mounted on the base plate located just after the premixing tube. Both the premixing tube and the liner were made of quartz to provide optical access. A flange made of quartz and having a hole 50 mm in diameter was located just after the quartz liner and used as a contraction. The flow had a high axial velocity at the centerline of the premixing tube. Under premixed operating conditions, the fuel was injected upstream of the swirl generator. An almost complete mixing of air and fuel had been achieved before the mixture entered the combustion chamber. An additional fuel line was coupled with the upper flange, where the liner was sitting, for supplying fuel to create a pilot flame. However, no pilot flame was used in the current investigations.

4.7 Atmospheric pressure test rig

All of the burners that were investigated were installed in an atmospheric pressure test rig at Lund University. A sketch of the test rig is shown in Fig. 4.9. It is equipped with controls for monitoring and operating the burners under different operating conditions. A high volume of air supply is provided by the two blowers (Rietschle SAP 300) and the range of the mass flow of air for two of the blowers is from 0 to 110 g/s when no combustion takes place. The Eldridge MPNH-8000 thermal mass flow meters mounted downstream of the blowers are used to monitor the mass flows of air. The flow of air is controlled by adjusting the motor speed of the blowers. There are two online heaters (Leister) located just after the mass flow meters for heating the bulk air up to 650 K. After passing through these, the bulk air-flow passes through the plenum over a series of meshes to break up the large flow structures. Fuel can be supplied to the burners from both the gas cylinder and the central gas network. There are arrangements for supplying fuel and air separately to the RPL section of the prototype 4th generation DLE burner. The RPL air can be preheated up to 650 K by using an extra heater. The air flow to the RPL and the fuel flows to all of the various burners are controlled by using Alicat Scientific mass flow controllers

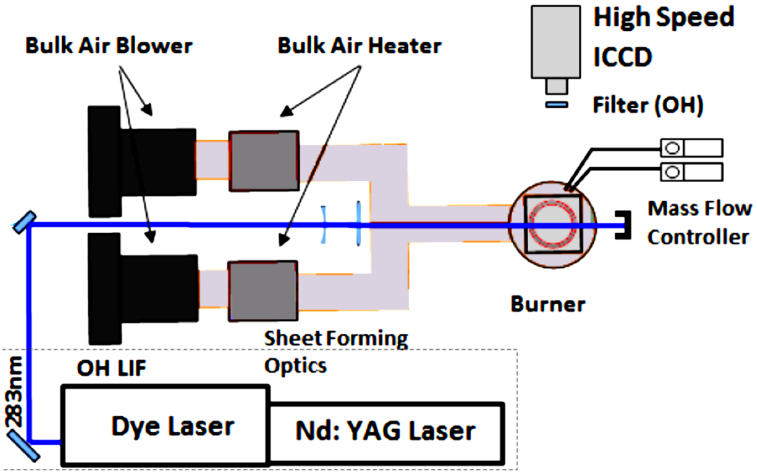

Figure 4.9: A schematic diagram of the measurement arrangements used in the laboratory.

Chapter 5

Applications and results

The experimental observations presented here are mainly from Papers I-VII included in the thesis. Certain unpublished works by the author are also included. The chapter is divided into three sections. In the first section, 5.1, the flame investigations performed on the prototype 4th generation DLE burner are discussed. In section 5.2, the studies of the hysteretic behavior of flashback and flash-forward in the TARS burner are presented. In the last section, 5.3, the experimental observations performed on the flame of the CECOST laboratory-scale swirling burner are discussed.

5.1 Flame investigations of the prototype 4th generation DLE burner

The prototype 4th generation DLE burner, described in section 4.6.1, has three sections with flexibilities to vary equivalence ratio in each of the sections separately. Different investigations were performed on this burner within the framework of the thesis concerning the development of the Siemens SGT750 gas turbine burner and are presented in Papers I-IV.

5.1.1 Flame investigation of the central pilot body

Lean premixed combustion in stationary gas turbines is a widely accepted approach that can provide low NO_X and CO values under a wide range of operating conditions. However, the lean premixed mode of the operation may create the risk of various unstable conditions, such as thermoacoustic instabilities, poor combustion efficiency and local flame extinction [5]. The inclusion of a diffusion pilot flame in the burner can help to stabilize the lean premixed combustion that takes place [6]. However, this also increases the production of NO_X. In order to retain the combustion stability and reduce the NO_X production, a premixed pre-chamber combustor can be used along with the pilot [71]. It can improve the lean blowout characteristics by supplying radicals that arise from the products and heat to the other burner sections for holding the main flame. The prototype 4th generation DLE burner also has a center pilot body or pre-combustor termed the RPL with a pilot section. The flame at the RPL exit was investigated at atmospheric pressure conditions while varying the equivalence ratio, residence time, and co-flow temperature employing OH-PLIF and high-speed chemiluminescence imaging. The flame chemiluminescence data provided information regarding the size and shape of the flame, whereas OH-PLIF images were used to identify the reaction zone and post-flame regions at locations defined by a laser sheet. Downstream of the RPL exit, flame oscillations were observed and were analyzed applying proper orthogonal decomposition to high-speed chemiluminescence data. The results of these investigations are presented in Paper I.

In the investigations, the RPL section was detached from the prototype burner assembly and was mounted in an atmospheric pressure test rig at Lund University, using an adapter. The setup employed is shown in Fig. 5.1.

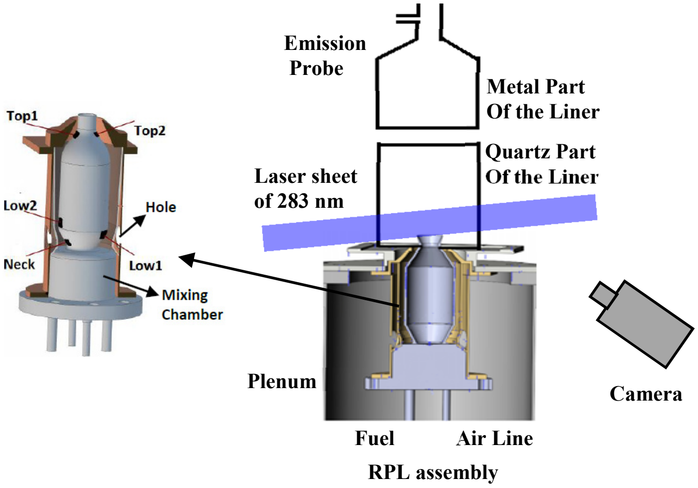

Figure 5.1: A schematic of the experimental setup and the RPL burner assembly.

The adapter throat has the same diameter as the intermediate sector (Pilot) of the prototype burner but is without swirl vanes. The investigations were carried out at two co-flow temperatures: 300 K and 650 K. A combustion chamber or liner 66 cm in length and having a 110 cm square cross section was positioned on top the burner assembly. The first 26 cm of this combustion liner was made of quartz to permit optical access to the post-burner region. The remaining 40 cm, including a contraction located at the outlet, was made of stainless steel. Since there was no access for optical measurements to investigate the combustion occurring inside the RPL, the flame was only investigated at the RPL exit. Five thermocouples were placed at various positions on the outer wall of the RPL for qualitative temperature comparisons to indicate about where combustion was taking place and discerned insofar as possible the location of the flame inside the burner volume.

OH-PLIF measurements were carried out by exciting the $Q1(8)$ transition of the OH radical with 283 nm laser sheet. An approximately 5 cm wide laser sheet was formed using sheet-forming optics and was passed through the mid-line of the burner exit. OH-PLIF and high-speed chemiluminescence images were collected using a CMOS camera. Details of the experimental setup are described in Paper I. For each flame condition, 1000 OH-PLIF single-shot images were collected at 10 Hz frequency, and 1000 chemiluminescence images were acquired at a sampling rate of 3 KHz.

For supplying fuel and air to the RPL, the mixing is achieved mainly due to the tangential entry of fuel and air into the mixing chamber. A high degree of swirl flow produces a recirculation zone at the expanding section located inside the RPL, and it is considered as a primary combustion zone of the RPL flame [72]. The location of this primary combustion zone inside the RPL changes with variation in the equivalence ratio, residence time and co-flow temperature. At a rich condition, the unburnt fuel comes out through the RPL exit together with products of the primary combustion, and the exhausts start secondary combustion downstream of the RPL exit at a lean fuel condition. Completion of the primary combustion taking place inside the burner depends upon the combustion rate as well as the residence time. If the combustion rate is able to overcome the residence time, complete combustion occurs inside the burner. Otherwise, the uninterrupted combustion extends past the RPL exit. The flame chemiluminescence and OH-PLIF images shown in Fig. 5.2 indicate how the flame behavior changes with variations in the equivalence ratio and residence time under non-preheated co-flow condition. The scaling of the probability density maps (PDMs) is the same for all the cases that are presented to show the differences in spatial signal distributions from one to another. In the images, the flow direction is upwards from the bottom. The diameter of the burner exit, d, normalizes the axial dimensions, and the origin is located at the center of the burner exit.

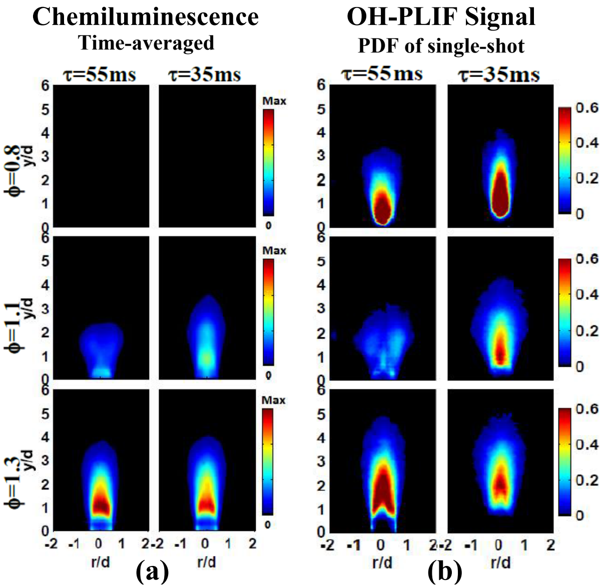

Figure 5.2: a) Time-averaged chemiluminescence signals, b) probability density maps (PDMs) of the OH-PLIF signal distributions at different operating cases under non-preheated co-flow condition.

At a lean equivalence ratio (ϕ = 0.8) under the non-preheated co-flow condition, for all residence times (τ), the temperature profile obtained from the thermocouples located on the outer wall of the RPL indicates the primary combustion to occur close to the RPL burner throat. The OH molecules that are found outside the burner exit have either been generated inside the burner close to the burner throat or are the result of the uninterrupted combustion that extends past the burner exit. However, the chemiluminescence images indicate no secondary combustion to have occurred outside the burner exit. Under the non-preheated co-flow condition, at ϕ = 1.1, close to stoichiometry, τ = 55 ms, the laminar flame speed increases. Consequently, the primary flame moves close to the burner entrance and reaches near to completion before exiting the RPL nozzle. Most of the intermediate OH radicals have completed their reactions, the remaining ones escaping together with the fuel-rich exhausts. Secondary combustion occurs then downstream of the burner under very lean conditions and a diffuse manner, the OH-PLIF signals thus being weak. At a rich condition, ϕ = 1.3, the temperature profile indicates the primary combustion to start close to the burner throat, such as in a ϕ = 0.8 case. However, at the fuel-rich condition, a greater amount of unburned fuel escapes the burner exit together with the exhaust gases or with the uninterrupted combustion. Oxygen from the co-flow needs more time then to blend with the unburned fuel to dilute the mixture to a level below the rich combustion limit. Thus, the ignition is delayed there, a secondary combustion occurring in a diffuse-like manner. The flame also becomes lifted above the burner exit and stabilizes downstream of the nozzle. With the decrease in residence time for all of the equivalence ratios, less time is available for combustion inside the burner to be completed. As a result, the flame moves downstream, and the OH distribution becomes stronger.

When the co-flow is pre-heated, this prevents a quenching effect from occurring through its reducing heat loss through the wall of the burner. It changes the flame and OH distributions as compared with the non-preheated co-flow conditions. Under the preheated co-flow condition, the primary combustion stabilizes near to the entrance of the RPL for most of the operating cases. Fig. 5.3 shows the flame chemiluminescence and OH-PLIF images for preheated co-flow cases.

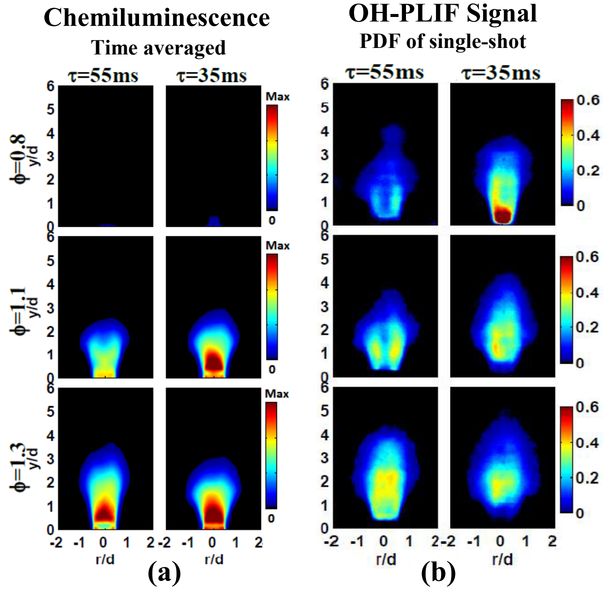

Figure 5.3: a) Time-averaged chemiluminescence signals, b) probability density maps (PDMs) of the OH-PLIF signal distributions at different operating cases under preheated co-flow condition.

Most of the operating conditions investigated show similar OH signal distributions at approximately the same position. Since this is a good indicator of flame stabilization, it reveals the importance of preheating the co-flow. The shape of the chemiluminescence signals is similar to that for the PDMs of the OH distributions for most of the cases studied, except under conditions in which $\phi = 0.8$. At $\phi = 0.8$ for each of the residence times, the chemiluminescence images indicate no secondary combustion to occur at the burner exit. Under both preheated and non-preheated co-flow conditions, fluctuations in combustion were observed. Proper orthogonal decomposition was applied to high-speed chemiluminescence data to investigate the flame dynamics that would be lost by standard time-averaging statistics. Further results and discussions of them are presented in Paper I.

5.1.2 Flame stabilization in the full burner configuration

Investigations of the prototype 4th generation DLE burner in the full configuration were carried out under atmospheric pressure conditions to better understand the flame stabilization and the changes in combustion that occur with alteration of the operating conditions in different sections of the burner. The operating conditions were altered by changing the equivalence ratios when methane was being used as fuel. OH-PLIF and chemiluminescence imaging were employed to study the local flame characteristics and formation of the reaction zones at the burner exit. The experimental setup is shown in Fig. 5.4 and described in Paper II. The OH-PLIF measurement was carried out by exciting $Q1(8)$ transition of the OH radical with a 5 cm wide laser sheet of 283 nm wavelength. An ICCD camera operated at 10 Hz sampling rate was used to collect the OH-PLIF signals. Both a high-speed (4.7 kHz) CMOS and a low-speed ICCD camera (10 Hz) were employed for obtaining the flame chemiluminescence images. The burner throat bulk velocity was set at 60 m/s during investigations.

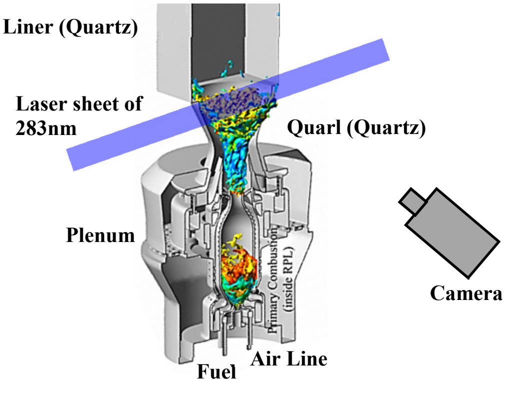

Figure 5.4: Schematic diagram of the experimental setup and of the full burner assembly.

The RPL was operated for both rich and lean mixtures except under stoichiometric condition to avoid both overheating and thermal damage to the RPL. The bulk air and the RPL air were preheated up to 650 K, whereas the fuel was not preheated. On the basis of the Pilot versus Main air split (21% and 79%, respectively), the fuel was injected into each section to maintain the same ϕ for both the Pilot and the Main stages. For changing the Pilot and the Main fuel split, the Pilot fuel ratio (PFR) was changed. The PFR is defined as:

$$\mathrm{PFR} = \frac{\text{Pilot fuel mass flow} \times 100\%}{\text{Main fuel mass flow} + \text{Pilot fuel mass flow}} \tag{5.1}$$

To be able to observe the contributions to the main flame from different sections of the burner, the fuel was released into the three sections in a stepwise manner, keeping the total air flow constant at a global $\phi = 0.5$. The operating conditions were: 1) RPL ($\phi = 1.2$), when only the RPL was provided with fuel, 2) RPL ($\phi = 1.2$) + Pilot ($\phi = 0.48$), when the RPL and the Pilot were provided with fuel, and 3) RPL ($\phi = 1.2$) + Pilot ($\phi = 0.48$) + Main ($\phi = 0.48$), when all three sections were provided with fuel. Fig. 5.5 shows photographs of the flame luminescence and Fig. 5.6 shows OH-PLIF signal distribution of the flames for each of these three conditions. The photographs, taken with a standard digital system camera, show the total extension of the flame, whereas the OH-PLIF signal distributions observed in the laser sheet provide information regarding the flame stabilization inside the Quarl. The diameter of the burner nozzle, *D*, normalizes the axial dimensions, the origin being located at the center of the burner exit. The lines that are overlaid show the position of the Quarl.

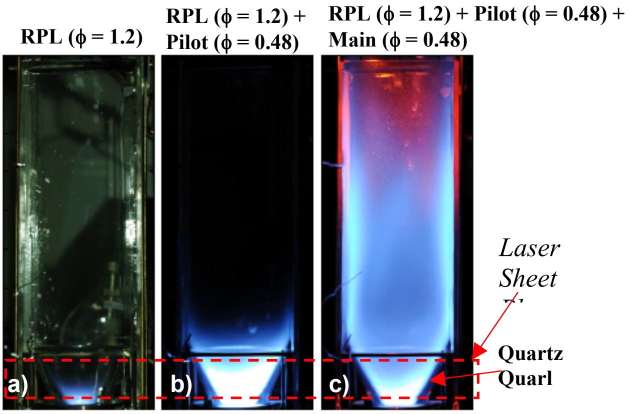

Figure 5.5: a-c show the photographs of the flames for the RPL, RPL + Pilot and RPL + Pilot + Main cases respectively. Global $\phi = 0.5$ and RPL $\phi = 1.2$.

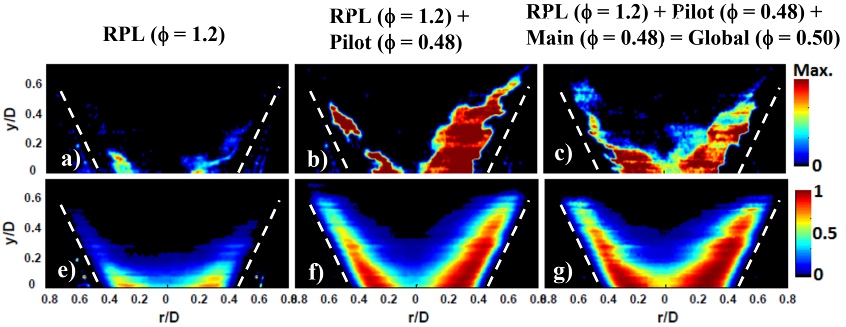

Figure 5.6: a-c show single-shot images and e-g show the PDMs of the OH-PLIF signal distributions of flames for the RPL, RPL + Pilot and RPL + Pilot + Main cases respectively. Global $\phi = 0.5$ and RPL $\phi = 1.2$.

In the full configuration, the RPL of the burner generates heat and free radicals to initiate ignition of the main flame. The residence time of the RPL combustor is sufficiently short so that a high concentration of the reacting atoms and radicals can contribute to the main flame to keep it within a stable combustion range. Both the photographs and OH radical distributions show there to be a small RPL secondary flame inside the Quarl in the case of the rich RPL ϕ. Under rich conditions, the residual fuel of the primary combustion that starts inside the RPL escapes through the RPL exit together with the primary combustion products and the active radicals. The flow of these fuel-rich exhausts interacts with the swirled Pilot airflow in the RPL-Pilot mixing tube, enhances the mixing, and initiates the secondary combustion. The secondary flame starts at the RPL exit and continues to expand in the diverging Quarl section due to imposed swirl.

The Pilot air stream enters the annular passage surrounding the RPL combustor through a series of holes. While passing through the annular passage, the pilot air picks up heat from the RPL combustor. For releasing fuel into the Pilot, the Pilot fuel and air start the reaction with the RPL hot exhausts in the RPL-Pilot mixing tube. The heat and exhausts from the RPL initiate the Pilot flame ignition. Since the Pilot fuel and air have only a short time to complete the mixing process before starting the interaction with the RPL exhausts stream, the mixing is not perfect, the combustion being initiated in a diffusion-like manner. The RPL-Pilot flame is confined mostly within the Quarl. The flame and the OH distribution become stronger as compared with the conditions of only the RPL flame being present.

In the Main section, the fuel has a longer residence time and distance available for mixing since the fuel there has been added sufficiently upstream. The Pilot-RPL mixtures that are combusted or partially combusted merge with the Main fuel-air mixtures at the burner throat. The Quarl, located just after the burner throat, expands and smooths both the flow field and the flame by means of a diverging cone. The CFD simulations of the flame stabilization are described in Paper III and ref. [73]. The photograph shown in Fig. 5.5(c) indicate that not all of the fuels from the Main section burn inside the Quarl. The main flame is anchored inside the Quarl and is elongated within the liner region. The OH signal distributions (shown in Fig. 5.6(c) and (g)) indicate the upstream progress of the full flame. The low signal intensities at the center of the OH distributions indicate the location of the central recirculation zone (CRZ) that is created by the swirling flow and is induced by vortex breakdown. The recirculation zone brings heat and radicals from the main parts of the flame zone towards the upstream mixing zone. The CRZ zone starts inside the Quarl section and continues to the liner region. In the photograph (Fig. 5.5(c)), the intense luminosity found inside the Quarl indicates the upstream position of the CRZ, the high degree of luminosity close to the liner wall suggesting the continuation of the CRZ there.

In Fig. 5.7(a), the changes in total flame length with a variation of the global ϕ are apparent. For increasing the global ϕ towards stoichiometry, the flame speed increases, and the flame shortens and moves upstream. Fig. 5.7(b) shows 2D OH-PLIF images for global ϕ = 0.46 and 0.60 at constant RPL ϕ = 1.4 and PFR = 21%.

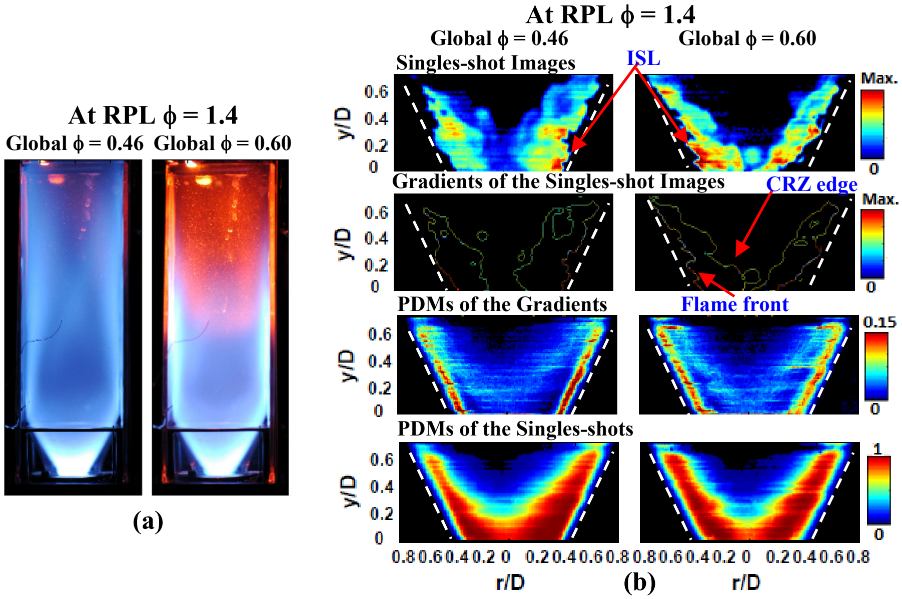

Figure 5.7: Flame images: (a) photographs of the full flame inside the liner (b) OH-PLIF images of different global ϕ (the unburned reactant is located between the Quarl wall and the flame).

The shear layer formed between the recirculation zone and the fresh reactant mixtures is termed the inner shear layer (ISL). The flame is stabilized in ISL inside the Quarl. The strongest gradients of the OH-PLIF signal, located near the Quarl wall, indicate the flame fronts. Here, the OH is produced in the reaction zone and eventually decreases towards the region of weak signals (the post-flame region) due to the short lifetime of the OH and its dilution by recirculating air and combustion products. The semi-strong gradients indicate the boundary layers between the RPL-Pilot stream and the CRZ. The boundary layer is termed the CRZ edge. PDMs based on the gradients can indicate fluctuations of the flame fronts and CRZ edges. With an increase in the global ϕ, the CRZ edge moves upstream, which indicates the flame-anchoring position to move upstream too. For increasing the RPL ϕ in the full burner configuration, the effect on the main flame is observed mostly inside the Quarl section. The increase in the RPL ϕ moves the flame stabilization zone downstream. Also, for increasing the PFR at a constant global ϕ, the total extension of the flame shortens, and the flame stabilization zone moves upstream. Further information regarding the experiments and the results obtained can be found in Paper II and III.

5.1.3 Effects of the burner geometry on the flame

For a lean and rich global ϕ under conditions with and without the Quarl, the OH signal distributions of flames are shown in Fig. 5.8. Under both conditions, the low signal intensities at the center of the OH distributions indicate that the flame stabilizes creating a CRZ which is caused by the swirl flow and induced by vortex breakdown. When the Quarl is not present, it makes a sudden expansion just after the burner exit. The flame gets more freedom then to expand radially and to stabilize, the flame thus becoming shorter. The CRZ becomes compact as well, and the flame stabilization moves downstream slightly. The most intense OH signals detected in flame (from single-shot and PDMs images) near the Quarl wall (under conditions with the Quarl) and downstream of the burner exit (under conditions without the Quarl) indicate the location of reaction zones. For increasing the global ϕ under both conditions of having a Quarl and no Quarl, the full flame shortens, and the CRZ becomes stronger, as indicated by intensification of the OH signal distribution (in PDMs of the OH-PLIF images) at the downstream ($y/D > 0.4$). In the presence of the Quarl, the OH distribution and the flame-anchoring position move upstream with an increase in the global ϕ due to the increase of the local laminar flame speed [74], whereas the opposite trend is observed when the Quarl is absent. Then both the OH distribution and the flame-anchoring position move downstream. In the case of a richer global ϕ ($\phi \geq 0.52$), the outer recirculation zones cannot be visible when the Quarl is present, but they can be observed when the Quarl is absent. Although the Quarl smooths the flow and directs the flame and flow, it limits the possibilities of their radial expansion. PDMs of the gradients (Figs. 5.8i-l) show that under all of the operating conditions both with and without the Quarl, the fluctuation of the flame fronts is less than that of the CRZ edges. The fluctuation of the CRZ edges spreads in both an axial and a radial direction. With an increase in the global ϕ, the CRZ edge moves upstream if the Quarl is present, whereas it shifts downstream if the Quarl is absent. The spreading of the fluctuations for the CRZ edges (both radially and axially) increases if the Quarl is absent. Further results are described in Paper IV.

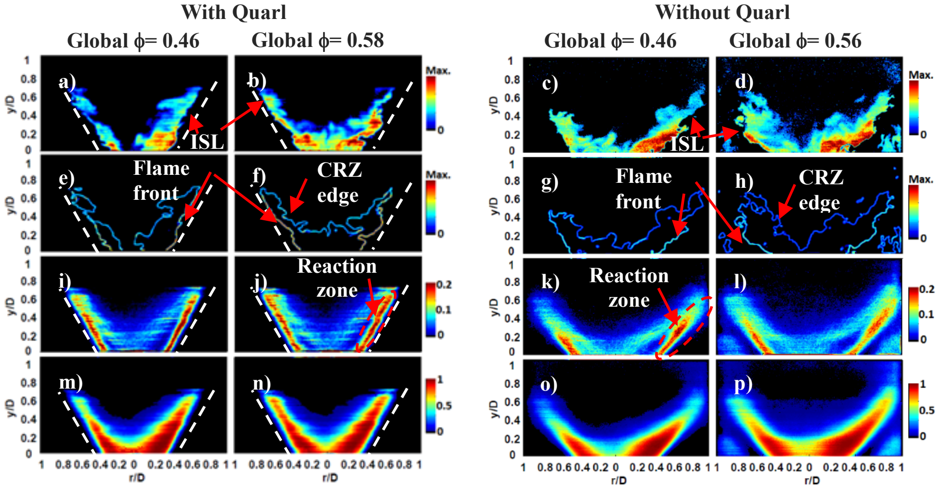

Figure 5.8: OH-PLIF images show how the OH distribution changes at a lean and rich global ϕ under conditions with and without Quarl. a-b show single-shot images for the global $\phi = 0.46$ and 0.58 under condition with Quarl and c-d show for the global $\phi = 0.46$ and 0.56 under condition without Quarl. e-h show the gradients of the single-shot images of a-d. i-l show the PDMs of OH gradients. m-p show the PDMs of single-shot images. The scales of x and y axes are the same for all images.

5.1.4 Effects of hydrogen enrichment on the methane flame

The availability of different gaseous fuel blends increases the need for gas turbines that can be operated in as flexible as possible with various types of fuels. Although lean premixed combustion is a well-known approach to reduce the production of thermal NO_X, it can lead to various types of unstable conditions [6]. Enrichment of more reactive species, such as hydrogen (H_2) in the fuel, can be a solution to mitigate such problems. H_2 enrichment of the CH_4 fuel extends the lean operation limits of combustion and decreases NO_X production, due to the lower temperatures of very lean flames. It also significantly reduces CO_2 production [75-77]. The laminar burning velocity of the H_2/CH_4 mixture increases as compared with that of the pure CH_4 due to the higher reaction rate, greater diffusivity and higher laminar burning velocity of H_2 [78]. Flame investigations were carried out on the prototype DLE burner for three different H_2/CH_4 fuel mixtures, having ratios (volumetrically) of 0/100, 25/75, and 50/50, without preheating of the fuels, while the Quarl was being kept. The global ϕ was varied within different ranges for each of the H_2/CH_4 fuel mixtures, keeping the RPL $\phi = 1.2$ constant. Fig 5.9 shows (a) photographs of the full flames and (b) OH distributions of the flames inside the Quarl, when the CH_4 fuel was enriched with 0 vol. %, 25 vol. %, and 50 vol. % of H_2 at a global $\phi = 0.42$. The photographs indicate there to be a substantial effect on the laminar flame speed for H_2 enrichment. The size of the flame shortens due to the increase in the laminar flame speed as well as the greater diffusivity and higher reaction rate of H_2.

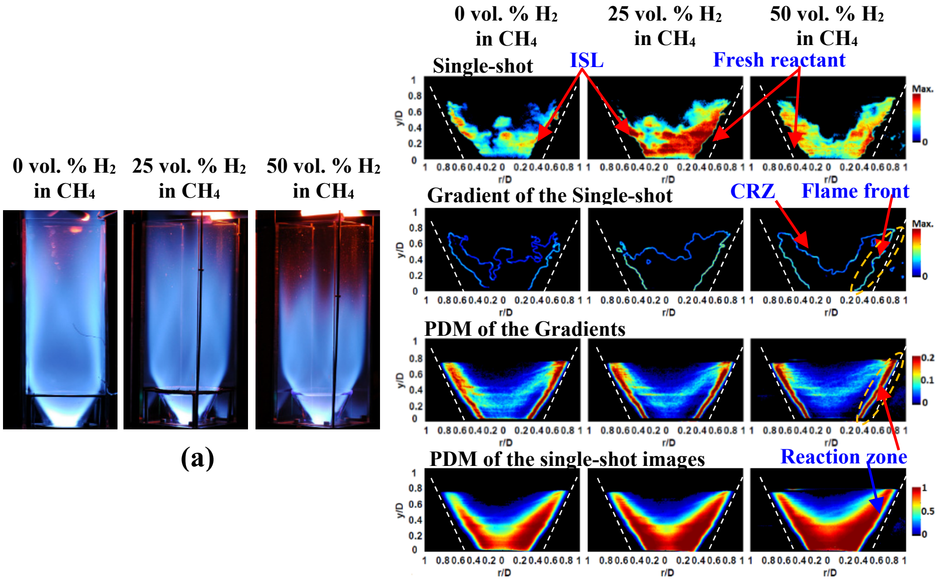

(a)

(b)

Figure 5.9: Flame images: (a) photographs of the full flame and (b) OH-PLIF images inside the Quarl for 0 vol. %, 25 vol. %, and 50 vol. % of H_2 enrichment in CH_4 fuel at a global $\phi = 0.42$.

For all cases, the low signal intensities at the center of the OH distributions indicate the locations of the CRZ that starts in the Quarl section and continues in the liner region. The ISL is formed between the CRZ and swirling fresh reactant mixtures. The highest gradients of temperature and OH radicals are located near the Quarl wall and indicating the reaction zones (shown in single-shots and PDMs of the OH gradients). The stabilization mechanism of the H_2 enchained flames using this burner can be found in a study [79] on the basis of CFD simulations and experimental investigations. For enriching the fuel with H_2, the production of the OH radicals in the flame increases, whereas the intermediate hydrocarbon (HC) fuel components decrease. Because of the high reaction rate and high burning velocity of H_2 fuel, H_2 combustion is mostly completed early in the upstream phase, whereas the products dilute the remaining fuel or intermediate HC radicals and take longer residence time for the combustion to be completed. Accordingly, the OH distribution inside the Quarl becomes thicker and stronger through CH_4 fuel enrichment by H_2. Higher amounts of the OH radicals are also produced by the RPL which contributes to the RPL-Pilot flame inside the Quarl. Although the OH signal distribution becomes stronger inside the Quarl, the luminosity of the flame there becomes weaker for the H_2 enrichment, as can be seen in the photographs. A similar trend can also be observed in the chemiluminescence images. When the amount of H_2 in the fuel mixtures increases, the production of the intermediate CH and C_2 radicals in the combustion is reduced. As a result, the blue-green luminescence (in the visible spectral region) of the flame caused by the electronic excitation of CH and C_2 becomes weakened. The PDMs of the gradients show that the fluctuation of the flame fronts is less than that of the CRZ edges in all cases. The fluctuation of the CRZ edges is found to be spread in both an axial and a radial direction. In enriching the flame with H_2, the CRZ edge moves downstream, which also indicates the flame-anchoring position to move downstream. The spreading of CRZ edge fluctuations increases with H_2 enrichment. Further information concerning the experiments and the results obtained can be found in Paper V.

5.2 Flashback in the TARS burner

In this work, the hysteretic behavior of flashback and flash forward in the TARS burner was investigated for methane and natural gas flames. The impacts of the relevant parameters including the Reynolds number, equivalence ratio, fuel type, combustion chamber geometry, preheating and mixing tube protrusions were investigated. The results of high-speed OH* chemiluminescence imaging and PIV measurements are presented in Paper VI. The flame and flow field of the TARS burner were also investigated experimentally employing PIV, laser Doppler velocimetry (LDV), and OH chemiluminescence imaging, and numerically by use of LES modeling [80-82].

The configurations of the TARS burner in the current investigation are described in section 4.6.2. OH-PLIF and CH_2O-PLIF measurements were carried out separately by exciting the OH and the CH_2O radicals with 283 nm and 355 nm laser light sheets that were 5 cm wide. For each flame condition, 1000 single-shot images were collected at 10 Hz frequency. High-speed PIV measurements were performed at 1 kHz frequency employing double-pulsed laser sheets of 527 nm wavelength to illuminate the flow field. In addition, the OH* chemiluminescence of the flame was recorded at 1 kHz sampling rate. All employed techniques were performed separately and described in Paper VI.

In the investigations carried out, two hysteresis cycles were identified at different Reynolds numbers for both CH_4 and natural gas flames. In the one cycle, the flashback was induced by increasing the equivalence ratio from a lean condition towards stoichiometry, whereas in the other cycle, the flashback was initiated by decreasing the equivalence ratio from a rich condition towards stoichiometry. These hysteretic behaviors are shown schematically in Fig. 5.10(a) for two Reynolds numbers. The hysteresis cycle at the left corresponds to lean conditions and that at the right to rich mixtures. The red lines correspond to a lower Reynolds number relative to the blue ones. Fig. 5.10(b) shows the dependency of the critical points on the Reynolds number in the case of methane. Both the lower, lean and higher, rich branches are plotted for both flashback and flash-forward. As the Reynolds number increases, the critical equivalence ratio increases on the lean branches and decreases on the rich branches. This behavior is related to the laminar flame speed, which increases as the equivalence ratio approaches unity. The two flashback branches (blue and red) merge at around equivalence ratio, $\phi = 1$, for Reynolds number, Re = 18000.

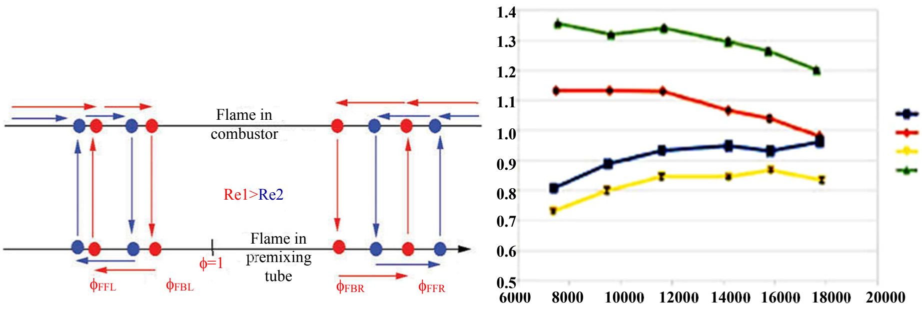

(a) **(b)**

Figure 5.10: a) Schematic diagram of the lean and rich hysteresis loops and the effects of changes in Reynolds number (Re). b) Summary of the critical equivalence ratios for flashback and flash forward for methane. The abbreviations denote the following: FBL, flashback at lean conditions; FBR, flashback at rich conditions; FFL, flash-forward at lean conditions; FFR, flash-forward at rich conditions.

The burner nozzle configuration was selected for studying the effects of the turbulence and boundary layer flashback mechanisms while avoiding the combustion-induced vortex breakdown and combustion instability related mechanisms. A strong non-swirling jet domination at the center of the flow field was achieved by removing the center swirler to eliminate the typical recirculation of the flow. Thus, the swirl number for the configuration was below the critical value of 0.7 [83]. The average axial and radial components of the flow field before and after flashback for a natural gas case (Re = 10500) are shown in Fig. 5.11. The velocity magnitudes are normalized by the average cold flow velocity in the premixing tube. Before flashback, while the flame is in the combustion chamber, two outer recirculation zones are apparent near the walls. Although there is no CRZ, a slight decay in the axial velocity along the center axis can be observed in the mean velocity profile. Downstream of the burner nozzle, there is a general outward motion, and the magnitude of the radial velocity component increases downstream. Flashback causes significant changes in the flow topology. The increase in temperature and the reduced density due to combustion in the premixing tube result in the flow to accelerate strongly. The axial velocity is significantly higher as compared with the pre-flashback levels. The axial velocity in the central region remains nearly unchanged, being like a jet, whereas the radial velocity becomes considerably lower.

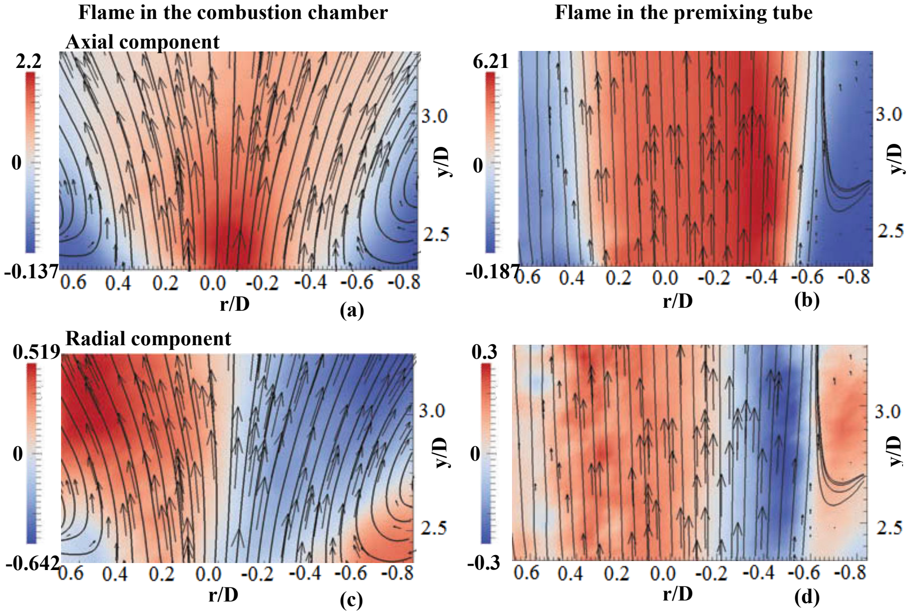

Figure 5.11: Average velocity field while the flame is in the combustion chamber (a, c) and in the premixing tube (b, d). Axial components (a, b) and radial components (c, d). Re = 10500.

Fig. 5.12 shows corresponding OH-PLIF and CH_2O-PLIF images in the combustor. Single-shots and PDMs of the OH and CH_2O signal distributions show that at a lean condition ($\phi = 0.59$), the flame is anchored inside the quartz combustion chamber for the flow of air-fuel mixtures. Increasing the equivalence ratio leads the flame to move upstream, due to the increase of the laminar flame speed. The OH and CH_2O signal distributions also indicate the absence of the CRZ and the presence of the two outer recirculation zones close to the walls before the flashback. When the flame is anchored at the burner nozzle after the occurrence of flashback, the jet flow of the combustion products exits the premixing tube outlet. Thus, a strong OH and a very weak CH_2O signal distribution are observed in the combustion chamber. OH radicals are formed in the reaction zone and transported to the hot post-flame region.

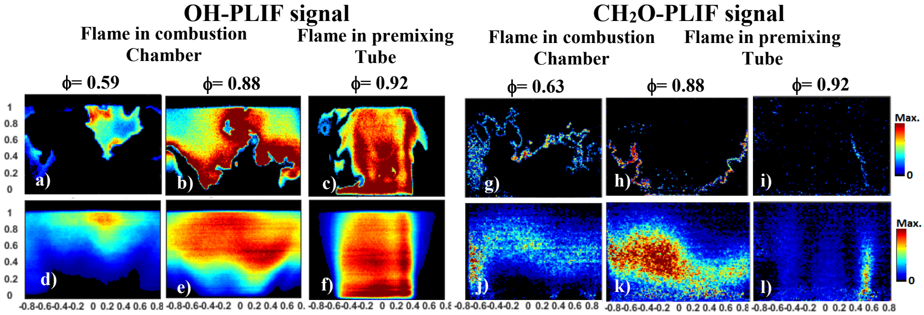

Figure 5.12: a) , b) & c) show single-shot OH-PLIF images; d), e) & f) show PDMs of OH-PLIF signal distributions; g) , h) & i) show CH_2O-PLIF images; j),k) & l) show PDMs of the CH_2O PLIF signal distributions. Re = 10500.

Both high-speed chemiluminescence images and flow field results support that the flashback initiates when the upstream tip of the flame penetrates into the mixing tube at the centerline, followed by the propagation of the flame more in-depth into the tube near the walls while rotating around them. Finally, the flashback is completed when the flame reaches the nozzle via the boundary layers of the mixing tube. The initial penetration at the centerline could be associated with a local combustion-induced vortex breakdown or be aided by the decay of the average axial velocity at that location. Such a transition from combustion-induced vortex breakdown to the flashback in the wall boundary layer is discussed in ref. [84]. Further information regarding the experiments and the results can be found in Paper VI.

5.3 Investigation of the CECOST laboratory-scale swirl burner

Experiments were performed on the CECOST laboratory-scale swirl burner to study the flame stabilization, lean blowout and flashback employing simultaneous OH-PLIF and CH_2O-PLIF as well as high-speed chemiluminescence imaging. The burner was mounted in an atmospheric pressure test rig at Lund University, a schematic diagram of the setup being shown in Fig. 5.13.

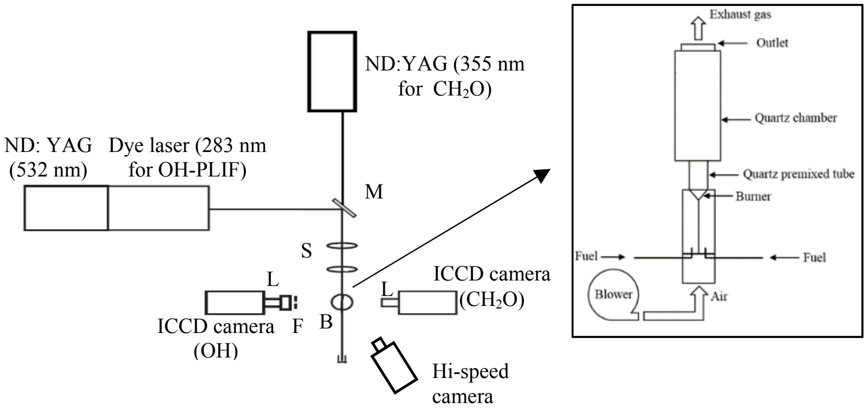

Figure 5.13: Experimental setup used for OH-PLIF, CH_2O-PLIF, and high-speed chemiluminescence measurements on the CECOST burner. The abbreviations denote the following: M, dichroic mirror; S sheet-forming optics; B, CECOST burner setup; L, camera lens; F, filter.

Simultaneous OH-PLIF and CH_2O-PLIF measurements were carried out by exciting the OH and CH_2O radicals with two overlapping 5 cm wide laser sheets of 283 nm and 355 nm, respectively. The time separation between the two laser pulses of 283 nm and 355 nm was 100 ns. The OH-PLIF and CH_2O-PLIF signals were detected using two ICCD cameras, each equipped with a Nikkor UV-lens. For the OH-PLIF signal, a combination of UG11 and WG305 long-pass filters was employed, whereas for the CH_2O signal a combination of two GG395 (Schott) filters was placed in front of the camera. For each flame condition, 1000 single-shot PLIF images were collected at 10 Hz frequency. The laser pulse energy for 355 nm was approximately 120 mJ, and for 283 nm, the pulse energy was varied between 14 mJ to 16 mJ during the measurements. A high-speed CMOS camera was used to acquire the OH* chemiluminescence images. For each flame condition, 1000 single-shot images were collected at 1 kHz frequency and with 200 μs of exposure time. For obtaining high-quality PLIF images, the flame in the premixing tube and combustion chamber were recorded separately. Strong reflections were caused by the 355nm (high power) laser sheet at the edges of the premixing tube, this affecting the CH_2O-PLIF measurements severely. Therefore, only OH-PLIF was utilized for capturing the flame structure present in the premixing tube, whereas the simultaneous OH-PLIF and CH_2O-PLIF results were used to study the flame structure present in the combustion chamber.

The effects of the equivalence ratio and the Reynolds number on the flame states were examined using natural gas as the fuel. Three main regimes, corresponding to lean blowout, steady flame and flashback were observed and are shown in Fig. 5.14. The lean blowout limit was found to be nearly invariant for all measured Reynolds numbers. At a lower Reynolds number ($Re \leq 10000$), the flashback was observed for increasing the equivalence ratio from a lean condition towards stoichiometry. This behavior is related to the laminar flame speed which increases as the equivalence ratio approaches unity. The flame was also observed to be anchored at the burner nozzle either under the same or higher equivalence ratio after the occurrence of the flashback. Within the range of the Reynolds numbers ($10000 < Re \leq 17000$), the critical equivalence ratio where the flashback occurred, was found to be higher for increasing the Reynolds number. After the flashback occurred, the flame was found to be unstable in the premixing tube and to not be anchored at the burner nozzle, even in the case of a further increase in the equivalence ratio. On the other hand, at a higher Reynolds number ($Re > 17000$), no flashback was observed for increasing the equivalence ratio, even close to the stoichiometry. At a higher Reynolds number, the increase in the bulk velocity plays a more important role in preventing the flashback and in stabilizing the flame in the chamber.

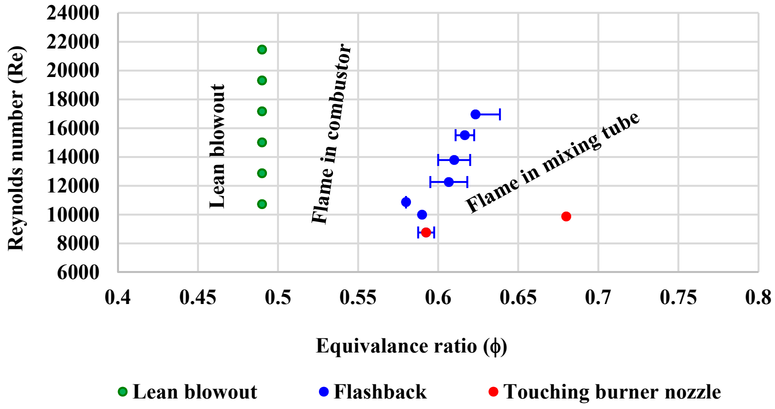

Figure 5.14: Reynolds number (Re) vs. equivalence ratio (ϕ) for different flame positions.

Fig. 5.15 presents time-averaged OH* chemiluminescence images and Fig. 5.16 shows OH-PLIF and CH_2O-PLIF signal distributions for ϕ = 0.52 and 0.60 at Re = 10000 and 20000. When the equivalence ratio is close to the lean blowout limit, the flame is observed to stabilize in the quartz combustion chamber. However, the low intensities of the OH* chemiluminescence and OH-PLIF signal distributions indicate the combustion to not be intense. In the combustion chamber, the flame stabilizes by creating a CRZ, as indicated by the low signal intensities at the center of the OH distributions. Along with the CRZ, two outer recirculation zones close to combustor walls are also observed. At the high Re = 20000, the flame size is reduced, and the CRZ becomes stronger in the combustor with an increase in the equivalence ratio. The flame fronts are indicated by the [OH] x [CH_2O] in the combustion chamber and by the gradients of the OH distribution in the premixing tube. The PDMs of the flame fronts indicate that the radial expansion of the flame in the combustion chamber remains almost the same for all ϕ at the high Reynolds number. In contrast, the expansion decreases with an increase in equivalence ratio at the low Reynolds number since the flame starts approaching in the mixing tube. At the low Re =10000, ϕ= 0.6, when the flame is anchored at the burner nozzle after the occurrence of flashback, the jet flow of the combustion products exits the premixing tube outlet. Therefore, strong OH-PLIF signal but very weak CH_2O-PLIF signal distributions are observed in the combustion chamber. Further information regarding the experiments and the results can be found in Paper VII.

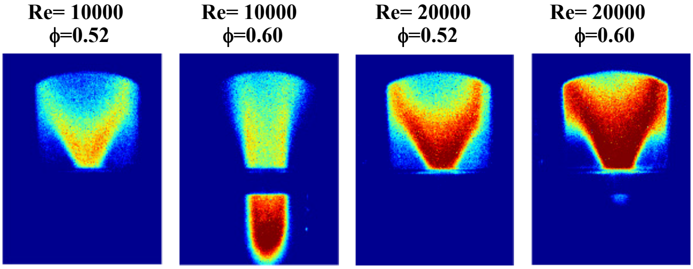

Figure 5.15: Time-averaged OH chemiluminescence images for ϕ = 0.52 and 0.60 at Re = 10000 and 20000.*

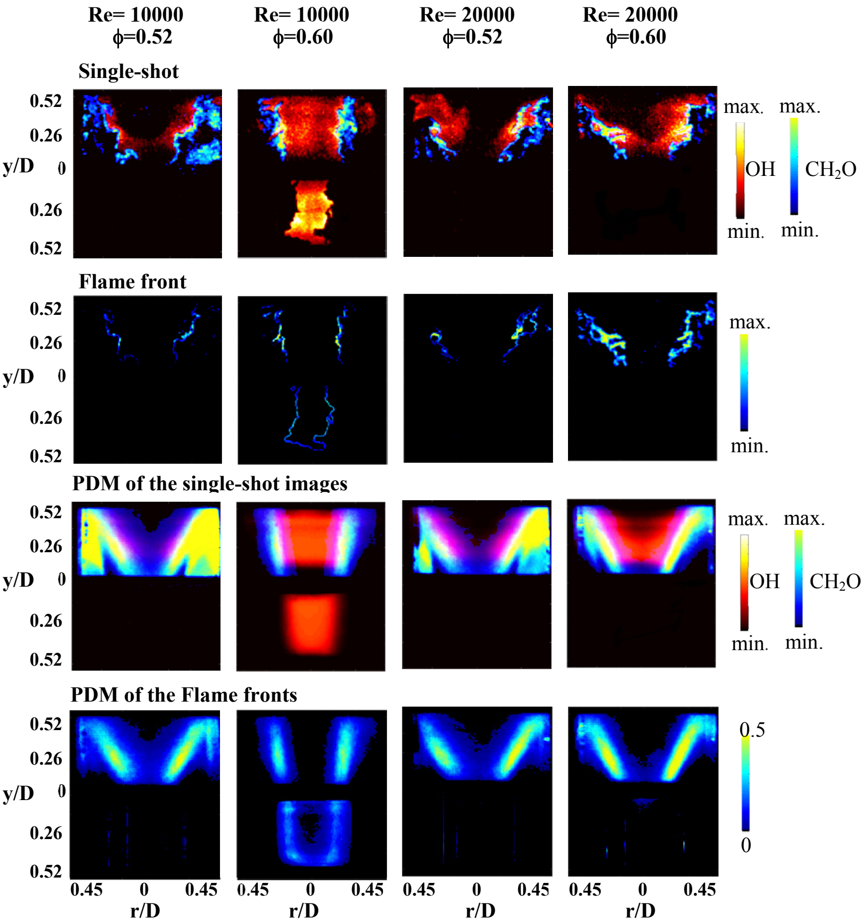

Figure 5.16: OH-PLIF and CH_2O-PLIF images for $\phi = 0.52$ and 0.60 at Re = 10000 and 20000.

Chapter 6

Summary and outlook

Gas turbines are operated at high Reynolds numbers and have complex flow fields as well as complex burner geometries. The construction of complicated burner geometries allows only limited optical access and provides only a certain degree of flexibility in regard to possible geometric changes. Therefore, investigations of these burners employing various advanced optical measurement techniques are challenging. A large part of the thesis involves experimental studies of a downscaled prototype 4th generation dry low emission (DLE) burner which concerns the development of the Siemens SGT-750 gas turbine burner. Experiments were carried out to study the flame and emissions under atmospheric pressure conditions, while varying different parameters in the three sections of the burner, changing the burner geometry, and altering the fuel composition. Planar laser-induced fluorescence (PLIF) of OH radicals as well as flame chemiluminescence imaging were employed, and emissions were sampled for studying the flame and combustion. The thesis also includes results of the experiments that were performed on two laboratory-scaled burners: a TARS and a CECOST swirl burner. These can simulate the characteristics of a gas turbine burner regarding both the fuel injection and flame stabilization. The flame investigations of these burners were performed employing OH-PLIF, CH_2O-PLIF, high-speed OH* chemiluminescence imaging and particle image velocimetry (PIV).

The central pilot body (RPL) of the DLE burner was investigated while varying the equivalence ratio, residence time, and co-flow temperature. It is found that under both the preheated and non-preheated co-flow conditions at lean equivalence ratios, the primary combustion starts early inside the RPL. If the combustion rate is able to overcome the residence time, complete combustion occurs inside the burner. Otherwise, the uninterrupted combustion extends past the RPL exit. Whereas under rich conditions, the residual fuel of the primary combustion that starts inside the RPL, escapes through the RPL exit together with the primary combustion products or with the uninterrupted combustion, and a secondary combustion is subsequently initiated downstream of the RPL exit at a leaner condition and in a diffusion-like manner. Under the preheated co-flow conditions, the flame stabilizes at the same position for most of the investigated operating cases. Since this is a good indicator of the flame stabilization, it reveals the importance of the preheating co-flow conditions.

The downscaled prototype DLE burner was investigated in a full burner configuration to study how the different sections of the burner interact with one another and affect the main combustion under various operating conditions. It is found that the RPL and Pilot flame are mostly confined within the Quarl region. The main flame is anchored inside the Quarl and extends within the liner region. The main flame is established through a swirl-induced central vortex breakdown phenomenon. The Pilot-RPL flame plays an essential role in the stabilization of the main flame. When the RPL equivalence ratio is increased, the flame stabilization region moves downstream of the burner exit. In contrast, the flame stabilization region moves upstream for increasing the global equivalence ratio and for increasing the Pilot fuel ratio at a particular global equivalence ratio.

Significant changes in the flame characteristics were observed in the case of sudden expansion at the prototype DLE burner exit when the geometry was changed by removal of the Quarl, as compared with the condition under which the Quarl was present. Both with and without the Quarl, the flame stabilizes creating a central recirculation zone, which is caused by the swirl flow and is induced by the vortex breakdown. When the Quarl is absent, the flame gets more freedom to expand radially and to stabilize, and therefore, the flame becomes shorter. The central recirculation zone becomes compact as well as the flame stabilization moves slightly downstream. In the case of a richer global equivalence ratio ($\phi \geq 0.52$), the outer recirculation zones cannot be visible when the Quarl is present, but they can be observed when the Quarl is absent.

Flame investigations were carried out for three different H_2/CH_4 fuel mixtures, having ratios (volumetrically) of 0/100, 25/75, and 50/50, without preheating of the fuel and the Quarl being present. The characteristics of the flames are affected by hydrogen enrichment. The size of the flame shortens due to the increase of the laminar flame speed as well as the higher diffusivity and the reaction rate of H_2. The flame stabilization zone moves further downstream of the burner exit. At a particular global equivalence ratio for altering the RPL and the Pilot equivalence ratio, the changes that occur in the CH_4 flame and the H_2 enriched CH_4 flame are similar.

The hysteretic behavior of flashback and flash-forward was investigated on the methane and natural gas flames of the Triple Annular Research Swirler (TARS) burner. The swirl number of the burner was minimized in these studies to prevent vortex breakdown. The effects of the turbulence and boundary layer flashback mechanisms were investigated. Two hysteresis loops are identified both for flashback and flash-forward, one for lean mixtures and the other for rich mixtures. The equivalence ratios at which rich and lean flashbacks occur, approach stoichiometry for increasing the Reynolds number. On the average, flashback events under lean conditions are found to be significantly slower than the same events under rich conditions, and than flash-forward events. Confinement effects are found to be less critical on both flashback and flash-forward.

Finally, experimental studies performed on the flame of the CECOST laboratory-scale swirl burner showed three regimes corresponding to lean blowout, steady flame, and flashback. The lean blowout limit was found to be nearly invariant for all measured Reynolds numbers. On the other hand, the flashback was found to approach around equivalence ratio (ϕ = 0.6) at lower Reynolds numbers and at higher equivalence ratios when the Reynolds number was increaed up to Re = 17000. With a further increase in the Reynolds number, no flashback was observed, even when the equivalence ratio was increased close to stoichiometry. At higher Reynolds numbers (Re > 17000), the increase in the bulk velocity played a more important role in preventing the flashback and in stabilizing the flame within the combustion chamber. There, the flame stabilizes by creating central recirculation and outer recirculation zones. At these higher Reynolds numbers, the flame size is reduced, and the central recirculation zone becomes stronger inside the combustion chamber with an increase in the equivalence ratio.

6.1 Future considerations

In the thesis work, all of the experimental investigations were performed on gas turbine related burners under atmospheric pressure conditions. However, in a real gas turbine, combustion takes place under much higher pressures. Pressure has significant effects on combustion characteristics due to the changes in heat loss, density, flame thickness, etc. Thus, investigations need to be performed under elevated pressure conditions along with atmospheric pressure conditions to obtain more information and better insight.

Investigating combustion instabilities, additional pressure and temperature transducers along with high-speed imaging techniques can provide a better understanding.

Different laser-based techniques need to be employed for not only qualitative analysis but also quantitative studies. Quantitative measurements of different intermediate species concentrations and temperature distributions are extremely advantageous.

The formation of a wider laser sheet is required to illuminate the larger areas of the combustion. For creating such a laser sheet having an even energy distribution, a high power laser system can be employed. The utilization of different PLIF measurement techniques at high repetition rates is also needed in order to understand the transient behavior of combustion phenomena.

References

1. IEA, *Key World Energy Statistics 2017*. IEA.
2. Turns, S., *2000, An Introduction to Combustion: Concepts and Applications, McGraw-Hill.* Boston.
3. Warnatz, J., P.-D.D.U. Maas, and R.W. Dibble, *Formation of nitric oxides*, in *Combustion*. 1996, Springer. p. 219-236.
4. Michaud, M.G., P.R. Westmoreland, and A.S. Feitelberg. *Chemical mechanisms of NO_X formation for gas turbine conditions*. in *Symposium (International) on Combustion*. 1992. Elsevier.
5. Lefebvre, A.H., *Gas turbine combustion: alternative fuels and emissions*. 2010: CRC press.
6. Lieuwen, T.C. and V. Yang, *Combustion instabilities in gas turbine engines(operational experience, fundamental mechanisms and modeling).* Progress in astronautics and aeronautics, 2005.
7. Gussak, L.A., et al., *Effect of adding individual combustion products on combustion of methane — Air mixture.* Bulletin of the Academy of Sciences of the USSR, Division of chemical science, 1973. **22**(9): p. 2128.
8. Carrera, A.M., M. Andersson, and H. Näsvall, *Experimental investigation of the 4th generation DLE burner concept: Emissions and fuel flexibility performance at atmospheric conditions.* ASME Paper No. GT2011-46387, 2011.
9. Sigfrid, I.R., et al. *Experimental investigation of lean stability limit of an prototype syngas burner for low calorific value gases*. in *ASME Conference Proceedings*. 2011.
10. Li, Z., et al., *Turbulence and combustion interaction: high resolution local flame front structure visualization using simultaneous single-shot PLIF imaging of CH, OH, and CH_2O in a piloted premixed jet flame.* Combustion and Flame, 2010. **157**(6): p. 1087-1096.
11. Eckbreth, A.C., *Laser diagnostics for combustion temperature and species*. Vol. 3. 1996: CRC Press.
12. Kohse-Höinghaus, K., *Laser techniques for the quantitative detection of reactive intermediates in combustion systems.* Progress in Energy and Combustion Science, 1994. **20**(3): p. 203-279.
13. Daily, J.W., *Laser induced fluorescence spectroscopy in flames.* Progress in energy and combustion science, 1997. **23**(2): p. 133-199.

14. SERIES, R.L., *Planar Optical Measurement Methods for Gas Turbine Components.* 1999.
15. Lantz, A., *Application of Laser Techniques in Combustion Environments of Relevance for Gas Turbine Studies*. 2012.
16. Richter, M., et al. *Real-time calibration of planar laser-induced fluorescence air-fuel ratio measurements in combustion environments using in situ Raman scattering*. in *Symposium (International) on Combustion*. 1998. Elsevier.
17. Barlow, R., R. Dibble, and R.P. Lucht, *Simultaneous measurement of Raman scattering and laser-induced OH fluorescence in nonpremixed turbulent jet flames.* Optics letters, 1989. **14**(5): p. 263-265.
18. Ehn, A., et al., *Fluorescence lifetime imaging in a flame.* Proceedings of the Combustion Institute, 2011. **33**(1): p. 807-813.
19. Bergano, N.S., et al., *Picosecond laser-spectroscopy measurement of hydroxyl fluorescence lifetime in flames.* Optics letters, 1983. **8**(8): p. 443-445.
20. Bechtel, J. and R. Teets, *Hydroxyl and its concentration profile in methane–air flames.* Applied Optics, 1979. **18**(24): p. 4138-4144.
21. Puri, R., et al. *Laser-induced fluorescence measurements of oh· concentrations in the oxidation region of laminar, hydrocarbon diffusion flames*. in *Symposium (International) on Combustion*. 1992. Elsevier.
22. Harrington, J.E. and K.C. Smyth, *Laser-induced fluorescence measurements of formaldehyde in a methane/air diffusion flame.* Chemical Physics Letters, 1993. **202**(3-4): p. 196-202.
23. Paul, P.H. and H.N. Najm. *Planar laser-induced fluorescence imaging of flame heat release rate*. in *Symposium (International) on Combustion*. 1998. Elsevier.
24. Clouthier, D. and D. Ramsay, *The spectroscopy of formaldehyde and thioformaldehyde.* Annual Review of Physical Chemistry, 1983. **34**(1): p. 31-58.
25. Metz, T., et al., *Fluorescence lifetimes of formaldehyde (H_2CO) in the Ã1A2→ X̃1A1 band system at elevated temperatures and pressures.* Spectrochimica Acta Part A: Molecular and Biomolecular Spectroscopy, 2004. **60**(5): p. 1043-1053.
26. Gabet, K., et al., *High-speed CH_2O PLIF imaging in turbulent flames using a pulse-burst laser system.* Applied Physics B, 2012. **106**(3): p. 569-575.
27. Duwig, C., et al., *High resolution imaging of flameless and distributed turbulent combustion.* Combustion and Flame, 2012. **159**(1): p. 306-316.
28. Libby, P.A. and F. Williams, *Turbulent flows involving chemical reactions.* Annual Review of Fluid Mechanics, 1976. **8**(1): p. 351-376.
29. Raffel, M., C.E. Willert, and J. Kompenhans, *Particle image velocimetry: a practical guide*. 2007: Springer Science & Business Media. 448.

30. Bahaa, E.S. and C.T. Malvin, *Fundamentals of photonics.* New York/A WILEY-INTERSCIENCE PUBLICATION, 1991.
31. Hult, J., et al., *Application of a high-repetition-rate laser diagnostic system for single-cycle-resolved imaging in internal combustion engines.* Applied optics, 2002. **41**(24): p. 5002-5014.
32. Löfström, C., H. Kaaling, and M. Aldén. *Visualization of fuel distributions in premixed ducts in a low-emission gas turbine combustor using laser techniques.* in *Symposium (International) on Combustion.* 1996. Elsevier.
33. Brackmann, C., et al., *Laser-induced fluorescence of formaldehyde in combustion using third harmonic Nd: YAG laser excitation.* Spectrochimica Acta Part A: Molecular and Biomolecular Spectroscopy, 2003. **59**(14): p. 3347-3356.
34. Bladh, H., J. Johnsson, and P.-E. Bengtsson, *Influence of spatial laser energy distribution on evaluated soot particle sizes using two-colour laser-induced incandescence in a flat premixed ethylene/air flame.* Applied Physics B: Lasers and Optics, 2009. **96**(4): p. 645-656.
35. Sadanandan, R., M. Stöhr, and W. Meier, *Simultaneous OH-PLIF and PIV measurements in a gas turbine model combustor.* Applied Physics B: Lasers and Optics, 2008. **90**(3): p. 609-618.
36. Kajava, T., H. Lauranto, and R. Salomaa, *Mode structure fluctuations in a pulsed dye laser.* Applied optics, 1992. **31**(33): p. 6987-6992.
37. Aikens, R.S., *Charge-Coupled Devices for Quantitative Electronic Imaging.* International Amateur-Professional Photoelectric Photometry Communications, 1991. **44**: p. 1.
38. Boyle, W.S. and G.E. Smith, *Charge coupled semiconductor devices.* Bell Labs Technical Journal, 1970. **49**(4): p. 587-593.
39. Sirovich, L., *Chaotic dynamics of coherent structures.* Physica D: Nonlinear Phenomena, 1989. **37**(1-3): p. 126-145.
40. Iudiciani, P., et al., *Proper orthogonal decomposition for experimental investigation of flame instabilities.* AIAA journal, 2012. **50**(9): p. 1843-1854.
41. Berkooz, G., P. Holmes, and J.L. Lumley, *The proper orthogonal decomposition in the analysis of turbulent flows.* Annual review of fluid mechanics, 1993. **25**(1): p. 539-575.
42. Smith, T.R., J. Moehlis, and P. Holmes, *Low-dimensional modelling of turbulence using the proper orthogonal decomposition: a tutorial.* Nonlinear Dynamics, 2005. **41**(1): p. 275-307.
43. Meyer, K.E., J.M. Pedersen, and O. Özcan, *A turbulent jet in crossflow analysed with proper orthogonal decomposition.* Journal of Fluid Mechanics, 2007. **583**: p. 199-227.

44. Hall, R.J. and P.A. Bonczyk, *Sooting flame thermometry using emission/absorption tomography.* Applied optics, 1990. **29**(31): p. 4590-4598.
45. Uchiyama, H., M. Nakajima, and S. Yuta, *Measurement of flame temperature distribution by IR emission computed tomography.* Applied optics, 1985. **24**(23): p. 4111-4116.
46. Daun, K.J., et al., *Deconvolution of axisymmetric flame properties using Tikhonov regularization.* Applied optics, 2006. **45**(19): p. 4638-4646.
47. Dasch, C.J., *One-dimensional tomography: a comparison of Abel, onion-peeling, and filtered backprojection methods.* Applied optics, 1992. **31**(8): p. 1146-1152.
48. Donbar, J.M., J.F. Driscoll, and C.D. Carter, *Reaction zone structure in turbulent nonpremixed jet flames—from CH-OH PLIF images.* Combustion and Flame, 2000. **122**(1): p. 1-19.
49. Cohen, H., G. Rogers, and H. Saravanamuttoo, *H.(r.) Saravanamutto.* Gas turbine theory, 1987.
50. Sigfrid, I.R., et al. *Parametric study of emissions from low calorific value syngas combustion, with variation of fuel distribution, in a prototype three sector burner*. in *ASME Conference Proceedings*. 2011.
51. Drake, M.C. and R.J. Blint, *Relative importance of nitric oxide formation mechanisms in laminar opposed-flow diffusion flames.* Combustion and Flame, 1991. **83**(1-2): p. 185-203.
52. Fenimore, C. *Formation of nitric oxide in premixed hydrocarbon flames*. in *Symposium (International) on Combustion*. 1971. Elsevier.
53. Konnov, A., G. Colson, and J. De Ruyck, *The new route forming NO via NNH.* Combustion and flame, 2000. **121**(3): p. 548-550.
54. Taamallah, S., et al., *Fuel flexibility, stability and emissions in premixed hydrogen-rich gas turbine combustion: Technology, fundamentals, and numerical simulations.* Applied Energy, 2015. **154**: p. 1020-1047.
55. Peters, N., *Turbulent combustion*. 2000: Cambridge university press.
56. Eichler, C.T., *Flame flashback in wall boundary layers of premixed combustion systems*. 2011: Verlag Dr. Hut.
57. Glassman, I., R.A. Yetter, and N.G. Glumac, *Combustion*. 2014: Academic press.
58. Seshadri, K. and N. Peters, *The inner structure of methane-air flames.* Combustion and Flame, 1990. **81**(2): p. 96-118.
59. Rott, N., *Note on the history of the Reynolds number.* Annual review of fluid mechanics, 1990. **22**(1): p. 1-12.
60. Poinsot, T. and D. Veynante, *Theoretical and numerical combustion*. 2005: RT Edwards, Inc.
61. Borghi, R., *Turbulent combustion modelling.* Progress in Energy and Combustion Science, 1988. **14**(4): p. 245-292.

62. Zhou, B., *Advanced Laser-based Multi-scalar Imaging for Flame Structure Visualization Towards a Deepened Understanding of Premixed Turbulent Combustion*. 2015.
63. Billant, P., J.-M. Chomaz, and P. Huerre, *Experimental study of vortex breakdown in swirling jets.* Journal of Fluid Mechanics, 1998. **376**: p. 183-219.
64. Stone, C. and S. Menon. *Combustion instabilities in swirling flows*. in *37th AIAA/ASME/SAE/ASEE Joint Propulsion Conference, AIAA 2001-3846*. 2001. Citeseer.
65. Jansohn, P., *Modern gas turbine systems: High efficiency, low emission, fuel flexible power generation*. 2013: Elsevier.
66. Walsh, P.P. and P. Fletcher, *Gas turbine performance*. 2004: John Wiley & Sons.
67. Whiddon, R., *Application of laser-based diagnostics to a prototype gas turbine burner at selected pressures*. 2014: Lund University (Media-Tryck).
68. Döbbeling, K., J. Hellat, and H. Koch. *25 Years of BBC/ABB/ALSTOM Lean Premix Combustion Technologies*. in *ASME Turbo Expo 2005: Power for Land, Sea, and Air*. 2005. American Society of Mechanical Engineers.
69. Sigfrid, I.R., et al. *Experimental and Reactor Network Study of Nitrogen Dilution Effects on NO_X Formation for Natural Gas and Syngas at Elevated Pressures*. in *ASME Turbo Expo 2013: Turbine Technical Conference and Exposition*. 2013. American Society of Mechanical Engineers.
70. Hodzic, E., *Analysis of flow dynamics and flame stabilization in gas turbine related combustors*. 2016.
71. Sigfrid, I.R., et al., *Influence of reactive species on the lean blowout limit of an industrial DLE gas turbine burner.* Combustion and Flame, 2014. **161**(5): p. 1365-1373.
72. Kundu, A., et al. *Operability and Performance of Central (Pilot) Stage of an Industrial Prototype Burner*. in *ASME 2015 Power Conference collocated with the ASME 2015 9th International Conference on Energy Sustainability, the ASME 2015 13th International Conference on Fuel Cell Science, Engineering and Technology, and the ASME 2015 Nuclear Forum*. 2015. American Society of Mechanical Engineers.
73. Kundu, A., et al. *Pilot-pilot interaction effects on a prototype DLE gas turbine burner combustion*. in *ASME Turbo Expo 2016: Turbomachinery Technical Conference and Exposition*. 2016. American Society of Mechanical Engineers.
74. Subash, A.A., et al. *Laser-Based Investigation on a Dry Low Emission Industrial Prototype Burner at Atmospheric Pressure Conditions*. in

ASME Turbo Expo 2016: Turbomachinery Technical Conference and Exposition. 2016. American Society of Mechanical Engineers.

75. Bell, S.R. and M. Gupta, *Extension of the lean operating limit for natural gas fueling of a spark ignited engine using hydrogen blending.* Combustion Science and Technology, 1997. **123**(1-6): p. 23-48.
76. Guo, H., et al., *The effect of hydrogen addition on flammability limit and NO_X emission in ultra-lean counterflow CH_4/air premixed flames.* Proceedings of the combustion institute, 2005. **30**(1): p. 303-311.
77. Schefer, R.W., D. Wicksall, and A. Agrawal, *Combustion of hydrogen-enriched methane in a lean premixed swirl-stabilized burner.* Proceedings of the combustion institute, 2002. **29**(1): p. 843-851.
78. Mandilas, C., et al., *Effects of hydrogen addition on laminar and turbulent premixed methane and iso-octane–air flames.* Proceedings of the Combustion Institute, 2007. **31**(1): p. 1443-1450.
79. Kundu, A., et al. *Fuel Flexibility of a Multi-Staged Prototype Gas Turbine Burner*. in *ASME Turbo Expo 2017: Turbomachinery Technical Conference and Exposition*. 2017. American Society of Mechanical Engineers.
80. Li, G. and E.J. Gutmark, *Effect of exhaust nozzle geometry on combustor flow field and combustion characteristics.* Proceedings of the Combustion Institute, 2005. **30**(2): p. 2893-2901.
81. Li, G. and E.J. Gutmark, *Boundary condition effects on nonreacting and reacting flows in a multiswirl combustor.* AIAA journal, 2006. **44**(3): p. 444.
82. Fureby, C., et al., *An experimental and computational study of a multi-swirl gas turbine combustor.* Proceedings of the Combustion Institute, 2007. **31**(2): p. 3107-3114.
83. Nestoil, P. and V. Island, *Vortex breakdown in a swirl-stabilized combustor.* Journal of Propulsion and Power, 2012. **28**(5).
84. Sattelmayer, T., C. Mayer, and J. Sangl, *Interaction of Flame Flashback Mechanisms in Premixed Hydrogen–Air Swirl Flames.* Journal of Engineering for Gas Turbines and Power, 2016. **138**(1): p. 011503.

Acknowledgements

This thesis is the outcome of a journey that started almost five years ago at the Division of Combustion Physics, Lund University. During this time, I met and worked with lots of people. I found a lot of friends and helping people. It was a fantastic period full of explorations and new experiences. At the end of this journey, I would like to thank and acknowledge all of those who made this possible through encouragements, supports, and joys.

At first, I would like to thank my main supervisor *Prof. Marcus Aldén* for introducing me to such an exciting field of research and believing in me to work on various research projects. I will always be grateful for your constant supports and encouragements.

I am very willing to show my gratitude to my co-supervisor *Robert Collin* for the time and effort you invested in me. You always had time for me to listen and advise me under any circumstance during these years. I am very thankful for your patience, positive attitude, and encouragements. Your supervisions and supports have been great importance to make this journey productive and stimulating.

I am thankful to *Prof. Jens Klingmann* for your guidance, ideas and all discussion regarding different combustion phenomena. I would like to thank *Prof. Xue-song Bai* for ideas and input during our discussions. Also thanks to *Atanu Kundu* who was the closest co-worker for the last four years. I think both of us were always conscious of keeping a good work environment even though we disagreed on different issues. Thank you for your cooperation during these years. Thanks to *Robert-Zoltán Szász* for helping me with all the technical and practical suggestions regarding research issues.

I am grateful to *Sven-Inge Möller* for your friendly support and all the useful discussions. You always encouraged and helped me to progress.

I am thankful to *Rutger Lorensson* for your helping attitude and tremendous support for solving various mechanical problems. Thanks also to *Igor Buzuk* for assistance in solving various electronics issues in the lab.

Thanks to *Prof. Per-Erik Bengtsson* for all the nice discussions we had.

Thanks to *Zhongshan Li* for all the motivating ideas and discussions.

I am grateful to *Minna Ramkull* and *Cecilia Bille* for helping me to deal with a huge number of paper works during these years and having lots of fascinating conversation.

It was very friendly and pleasant to share the office with *Ronald Whiddon* during the first one and half years and with *Jim Larsson* for the remaining period. Thanks to *Ronald Whiddon* for introducing me to the fluorescence lab and gas turbine burners. You have always been a good friend. Thanks to *Jim Larsson* for all the fun discussions and always helping me out with the Swedish language. I wish you all the best in the future. Thanks to *Dina Hot* for your support, encouragement and for being a nice friend. I am also thankful to *Panagiota Stamatoglou, Kajsa Larsson, Alexios Matamis, Erdzan Hodzic, Sandra Török, Gianluca Capriolo, Yogeshwar Nath Mishra, Anna-Lena Sahlberg* and *Manu Mannazhi* for being great friends and making the journey pleasant and exciting. Especial thanks to *Andreas Lantz* for always being excellent supportive and positive when you were in this Division and are in Siemens now. I would also like to thank *Fahed Abou Nada, Elin Malmqvist, Ludovica Luise, Moah Christensen, Joakim Jönsson, Ali Hosseinnia, Maria Ruchkina, Zhenkan Wang, Edouard Berrocal, Wubin Weng, Haisol Kim, Vladimir Alekseev,* and *Christoffer Pichler* for all the pleasant time. To my co-workers, *Xin Liu* and *Senbin Yu*- good luck! It was very nice to work with you.

I would also like to thank all currently and previously present persons from the Division not mentioned by name. You all have contributed to the friendly atmosphere at work, as well as during our numerous social activities.

I am grateful to *Mohammed Abdul Naium* for your constant encouragement and support.

I would like to take the opportunity as well to thank my great friends *Tayeb Husain, Kakali Adhikary, Saira Naim Shuchana, Afsana Haider Mohona, Israt Jahan, Mohammad Alif Arman, Shahriar Newaz* and *Manzur Kader, Shubhabrata Sen* for excellent support and fun time we have spent together during these years. Thanks to *Mahbubul Talukder Shafi* for all those times, you were there for my family during these years.

I truly appreciate *Daniel Loerstad* and *Jenny Larfeldt* for providing the opportunities to discuss regarding the combustion of Siemens burner.

I would like to thank the Swedish Energy Agency, Siemens Industrial Turbomachinery AB, GKN Aerospace Engine Systems Sweden AB, the Royal Institute of Technology through the Swedish research program TURBO POWER, and the Centre for Combustion Science and Technology, CECOST, for the financial support.

I am grateful to thank my sister, *Arjuda Ahamed Snigdha* and her husband, *Asaduzzaman Rasel*, for your support and believe in me. You have always tried to fill in lots of joy and happiness to my home in Bangladesh during all these years when I was mostly away.

Finally, I would like to direct my most profound gratitude to my parents, *Mohammed Mukshed Ali* and *Mrs. Rowshan Ara Khanam*, for your unconditional love, support and encouragement. *Mohammed Mukshed Ali*, you are and will always be the most important mentor and the key source of inspiration in my life. *Mrs. Rowshan Ara Khanam*, without your unlimited patience and sacrifice during the most important times of my life, I would never come so far. I would also like to show my gratitude to my beloved wife, *Alfi Shaharin*, for your enormous persistence, encouragement and endless support. You have always been at my side during not only the joyful, happiest moments but also the toughest days of my life. I am genuinely thankful to you.

Summary of papers

Paper I

Subash, A. A., Whiddon, R., Kundu, A., Collin, R., Klingmann. J., & Aldén, M., "Flame Investigation of a Gas Turbine Central Pilot Body Burner at Atmospheric Pressure Conditions Using OH PLIF and High-Speed Flame Chemiluminescence Imaging", *In Proceeding of the ASME Gas Turbine India Conference, 2015, GTINDIA2015-1212*

Investigations were carried out on the central pilot body of the Siemens prototype 4th generation DLE burner to investigate the flame behavior at atmospheric pressure conditions, using CH_4 as a fuel. The central pilot body or the RPL (rich-pilot-lean) plays a vital role in stabilizing the main flame, in a full burner configuration, preventing discontinuities in the flame during different operating conditions. The flame was studied at the RPL burner exit varying the equivalence ratio, residence time and co-flow temperature. Investigations were performed employing OH planar laser-induced fluorescence as well as high-speed chemiluminescence imaging. Changes in the RPL co-flow temperature and flow rate alter the flame stabilization. The flame dynamics were analyzed applying proper orthogonal decomposition to time-resolved chemiluminescence data. NO_X measurement was also performed to complement the measurements of different operating conditions.

I took part in the planning of the measurements, building the setup, and participated in all the experimental works. I was mainly responsible for performing the OH-PLIF experiment as well as post-processing of the OH- PLIF and chemiluminescence data. Whiddon R. was responsible for planning and deciding on the experimental parameters. Kundu A. was responsible for the emission measurements and analyzing the NO_X *emission data. As a lead author, I prepared the manuscript. Aldén M., Collin R., and Klingmann J. supervised the experiment and the writing of the manuscript.*

Paper II

Subash, A. A., Kundu, A., Collin, R., Klingmann. J., & Aldén, M., "Laser-Based Investigation on a Dry Low Emission Industrial Prototype Burner at Atmospheric Pressure Conditions", *In Proceedings of the ASME Turbo Expo 2016, Volume 4B: Combustion, Fuels and Emissions, GT2016-57242*

In this paper, investigations of the flame were performed on the prototype 4th generation DLE burner in full configuration under atmospheric pressure conditions using CH_4 as the fuel. The Planar laser-induced fluorescence of OH radicals and flame chemiluminescence imaging were employed to study the flame behavior as well as the location and stabilization of the flame during systematic stepwise changes in the equivalence ratios of three sections (RPL, Pilot, and Main) of the burner. During the experiment, it was also studied how the different sections of the burner interact with one another and how they affect the main flame at different operating conditions.

I took part in the planning of the measurements, building the setup, and participated in all the experimental works. I was mainly responsible for performing the OH-PLIF experiment. Kundu A. was responsible for deciding on the test-operating conditions, emission measurements and analyzing the NO_X emission data. I performed post-processing of the OH-PLIF and chemiluminescence data and prepared the manuscript. Aldén M., Collin R., and Klingmann J. supervised the experiment and the writing of the manuscript.

Paper III

Kundu, A., **Subash, A. A.,** Collin, R., & Klingmann. J., "Flame Stabilization and Emission Characteristics of a Prototype Gas Turbine Burner at Atmospheric Conditions", *In Proceedings of the ASME Turbo Expo 2016, Volume 4B: Combustion, Fuels and Emissions, GT2016-57336*

This paper is based on the same experimental studies presented in Paper II. The primary focus was to investigate the flame stability, operability and emission capability of the prototype 4th generation DLE burner for using CH_4 as the fuel. Along with the planar laser-induced fluorescence of OH and chemiluminescence imaging, the emissions of NO_X, CO, and UHC were measured to investigate combustion. Different points of instabilities (lean operation and burner staging effects) were identified, and possibilities for enhancement of the operability window were explored. Numerical analysis using FLUENT was carried out to understand the scalar and vector fields. A simplified chemical reactor network model was also developed for comparing the measured emission data with the model.

As a co-author, my contribution to this paper was to participate in the planning of the measurements, building the setup, and performing the experiments. I was mainly responsible for performing the OH-PLIF experiment and post-processing of OH-PLIF data. Kundu A. was responsible for deciding on the test-operating conditions, the CFD analysis, and the reactor modeling as well as analyzing the emission data. Kundu A. prepared the manuscript, to which I contributed with the part concerning OH measurement. Collin R. and Klingmann J. supervised the experiment and the writing of the manuscript.

Paper IV

Subash, A. A., Kundu, A., Collin, R., Klingmann. J., & Aldén, M., "Experimental Investigation of the Influence of Burner Geometry on Flame Characteristics at a Dry Low Emission Industrial Prototype Burner at Atmospheric Pressure Conditions", *In Proceedings of the ASME Turbo Expo 2017, Volume 4A: Combustion, Fuels and Emissions, GT2017-63950*

Laser-based investigations were performed on a prototype 4th generation DLE (dry low emission) burner under atmospheric pressure conditions to study the effects on the flame for changing the burner geometry. In the full burner configuration, a divergent conical section termed the Quarl is located after the burner exit for expanding the flow area and holding the flame. The flame shape, reaction zones, and post-flame regions of the flame were studied by use of the planar laser-induced fluorescence of OH and chemiluminescence imaging under conditions of using and not using the Quarl. The primary goal was to understand the effects of the Quarl on the flame.

I took part in the planning of the measurements, building the setup, and participated in all the experimental works. I was mainly responsible for performing the OH-PLIF experiment. Kundu A. was responsible for deciding on the test-operating conditions, emission measurements and analyzing the NO_X emission data. I performed post-processing of the OH-PLIF and chemiluminescence data and prepared the manuscript. Aldén M., Collin R., and Klingmann J. supervised the experiment and the writing of the manuscript.

Paper V

Subash, A. A., Kundu, A., Collin, R., Klingmann. J., & Aldén, M., "Hydrogen Enriched Methane Flame in a Dry Low Emission Industrial Prototype Burner at Atmospheric Pressure Conditions", *In Proceedings of the ASME Turbo Expo 2017, Volume 4A: Combustion, Fuels and Emissions, GT2017-63924.*

In this paper, optical investigations were performed to study the effects of H_2 enrichment on the CH_4 flame in a prototype 4th generation DLE burner under atmospheric pressure conditions. The flame was investigated for three different H_2/CH_4 mixtures having ratios (volumetrically) of 0/100, 25/75, and 50/50. The Planar laser-induced fluorescence of OH radicals together with flame chemiluminescence imaging were employed for studying the flame shape, reaction zones, and post-flame regions at the burner exit. Combustion emissions were also determined to observe the effects of H_2 enrichment on the NO_X level.

I took part in the planning of the measurements, building the setup, and participated in all the experimental works. I was mainly responsible for performing the OH-PLIF experiment. Kundu A. was responsible for deciding on the test-operating conditions, emission measurements and analyzing the NO_X emission data. I performed post-processing of the OH-PLIF and chemiluminescence data and prepared the manuscript. Aldén M., Collin R., and Klingmann J. supervised the experiment and the writing of the manuscript.

Paper VI

Szasz, R.Z., **Subash, A. A.,** Lantz, A., Collin, R., Fuchs, L., & Gutmark, E.J., "Hysteretic Dynamics of Flashback in a Low-Swirl Stabilized Combustor", *Journal Combustion Science and Technology Volume 189, 2017 - Issue 2.*

The hysteretic behavior of flashback and flash-forward was investigated on the flame of the triple annular research swirler (TARS) burner. In this investigation, the swirl number of the burner was minimized to prevent vortex breakdown, methane and natural gas being used as fuels. The effects of the turbulence and boundary layer flashback mechanisms were studied. The investigations were executed using high-speed OH* chemiluminescence and particle image velocimetry. The equivalence ratio was used to control flashback and flash-forward. The impact of relevant parameters consisting of the Reynolds number (Re), equivalence ratio, fuel type, combustion chamber geometry, preheating, and mixing tube protrusions were investigated.

I took part in the planning of the measurements, building the setup, and participated in all the experimental works. I was responsible for high-speed OH chemiluminescence imaging and post processing chemiluminescence data. Szasz R.Z. was responsible for deciding on the test-operating conditions and PIV measurements. Szasz R.Z. also post-processed the PIV data and prepared the manuscript. Lantz, A., Collin. R. and Fuchs. L. and Gutmark E.J. supervised the experiment and the writing of the manuscript.*

Paper VII

Yu, S., **Subash, A. A.,** Liu, X., Liu, X., Hodzic, E., Szasz, R.Z., Bai, X.S., Li, Z.S., Collin, R., Aldén, M., & Lörstad, D., "Numerical and Experimental Investigation of the Flame Structures in a New Lab-Scale Gas Turbine Swirl Burner", *ASME Turbo Expo 2018 (submitted)*

In this paper, experimental and numerical investigations were performed on a laboratory-scale swirl burner to study the flame stabilization, lean blowout, and flashback. Simultaneous OH-PLIF and CH_2O-PLIF, as well as high-speed chemiluminescence imaging, were employed to investigate the flame experimentally, whereas numerical studies on the reacting flow were performed employing Large-eddy Simulation (LES). The effects of the equivalence ratio and Reynolds number on the flame states were examined. It was found that with an increase in the Reynolds number, flashback became more difficult, this indicating the extension of the range in which for flame stabilization can be achieved.

I took part in the planning of the measurements, building the setup, and participated in all the experimental works. I was mainly responsible for performing the simultaneous OH-PLIF and CH_2O-PLIF experiment and the high-speed OH chemiluminescence imaging. Yu, S. was responsible for calculating the test-operating conditions, CFD analysis, reactor modeling and flame surface density (FSD) analysis. Liu, X., was responsible for post-processing the OH* chemiluminescence data. I performed post-processing of OH-PLIF and CH_2O-PLIF data. Yu, S. prepared the manuscript. Aldén M., Collin. R. and Bai, X.S. supervised the experiment and the writing of the manuscript.*